

Review and Assessment of Nanofluid Technology for Transportation and Other Applications

Energy Systems Division

About Argonne National Laboratory

Argonne is a U.S. Department of Energy laboratory managed by UChicago Argonne, LLC under contract DE-AC02-06CH11357. The Laboratory's main facility is outside Chicago, at 9700 South Cass Avenue, Argonne, Illinois 60439. For information about Argonne, see www.anl.gov.

Availability of This Report

This report is available, at no cost, at <http://www.osti.gov/bridge>. It is also available on paper to the U.S. Department of Energy and its contractors, for a processing fee, from:

U.S. Department of Energy

Office of Scientific and Technical Information

P.O. Box 62

Oak Ridge, TN 37831-0062

phone (865) 576-8401

fax (865) 576-5728

reports@adonis.osti.gov

Disclaimer

This report was prepared as an account of work sponsored by an agency of the United States Government. Neither the United States Government nor any agency thereof, nor UChicago Argonne, LLC, nor any of their employees or officers, makes any warranty, express or implied, or assumes any legal liability or responsibility for the accuracy, completeness, or usefulness of any information, apparatus, product, or process disclosed, or represents that its use would not infringe privately owned rights. Reference herein to any specific commercial product, process, or service by trade name, trademark, manufacturer, or otherwise, does not necessarily constitute or imply its endorsement, recommendation, or favoring by the United States Government or any agency thereof. The views and opinions of document authors expressed herein do not necessarily state or reflect those of the United States Government or any agency thereof.

Review and Assessment of Nanofluid Technology for Transportation and Other Applications

by
W. Yu, D.M. France, S.U.S. Choi, and J.L. Routbort
Energy Systems Division, Argonne National Laboratory

work supported by the
Office of FreedomCAR and Vehicle Technologies
U.S. Department of Energy, Office of Energy Efficiency and Renewable Energy

April 2007

Table of Contents

| | |
|---|----|
| Nomenclature | 4 |
| Abstract | 6 |
| 1. Introduction | 6 |
| 2. Nanofluid Research | 8 |
| 3. Production of Nanoparticles and Nanofluids | 9 |
| 4. Barriers and Challenges to the Commercial Production of Nanofluids | 10 |
| 4.1. Two-Step Process | 10 |
| 4.2. One-Step Process | 10 |
| 4.3. Other Processes | 11 |
| 5. Experimental Research on Nanofluid Thermal Conductivity | 13 |
| 5.1. Effect of Particle Volume Concentration | 13 |
| 5.2. Effect of Particle Material | 15 |
| 5.3. Effect of Particle Size | 16 |
| 5.4. Effect of Particle Shape | 18 |
| 5.5. Effect of Base Fluid Material | 19 |
| 5.6. Effect of Temperature | 19 |
| 5.7. Effect of Additives | 21 |
| 5.8. Effect of Acidity (pH) | 22 |
| 6. Experimental Research on Nanofluid Heat Transfer | 23 |
| 6.1. Heat Transfer Enhancement in Laminar Flow | 23 |
| 6.2. Heat Transfer Enhancement in Turbulent Flow | 26 |
| 6.3. Heat Transfer Enhancement in Pool Boiling | 27 |
| 6.4. Critical Heat Flux Enhancement in Pool Boiling | 28 |
| 7. Experimental Research on Nanofluid Erosion | 31 |
| 8. Theoretical Modeling of Nanofluids | 32 |
| 8.1. Density and Specific Heat | 32 |
| 8.2. Thermal Conductivity | 32 |
| 8.2.1. Effect of Nanoparticle-Matrix Interfacial Layer | 33 |
| 8.2.2. Effect of Nanoparticle Brownian Motion | 35 |
| 8.2.3. Effect of Nanoparticle Cluster/Aggregate | 36 |
| 8.2.4. Nanofluids Containing Carbon Nanotube Particles | 37 |
| 8.3. Viscosity | 38 |
| 8.4. Heat Transfer Coefficient | 39 |
| 8.5. Simulation | 39 |

| | |
|--|----|
| 9. Applications of Nanofluids | 41 |
| 9.1. Transportation | 41 |
| 9.2. Electronics Cooling..... | 42 |
| 9.3. Defense | 42 |
| 9.4. Space | 43 |
| 9.5. Nuclear Systems Cooling..... | 43 |
| 9.6. Biomedicine | 43 |
| 9.7. Other Applications | 43 |
| 10. Concluding Remarks and Future Work | 45 |
| Appendix A. Compilation of Experimental Data on Nanofluids | 47 |
| Table 1. Thermal Conductivity Enhancements..... | 48 |
| Table 2. Single-Phase Heat Transfer Enhancements | 52 |
| Table 3. Pool-Boiling Heat Transfer Enhancements | 54 |
| Table 4. Pool-Boiling Critical Heat Flux Enhancements..... | 55 |
| Appendix B. Mathematical Models of Nanofluids | 56 |
| Table 5. Models of Effective Thermal Conductivity | 57 |
| Table 6. Models of Effective Viscosity | 60 |
| Table 7. Models of Effective Heat Transfer Coefficient | 62 |
| References..... | 63 |

Nomenclature

| | |
|------------|--|
| a, b, c | ellipsoid semi-axes, $a \geq b \geq c$ |
| CHF | critical heat flux, W/m^2 |
| C_p | specific heat, J/kgK |
| c_p | particle dependent parameter |
| D | diameter, m |
| D_h | hydraulic diameter, m |
| d | depolarization factor |
| d_f | fractal dimension |
| f | friction factor |
| G | mass flux, kg/m^2s |
| g | gravitational acceleration, m/s^2 |
| h | heat transfer coefficient, W/m^2K |
| k | thermal conductivity, W/mK |
| k_a | aggregate conductivity, W/mK |
| k_B | Boltzmann constant, $k_B = 1.3807 \times 10^{-23} J/K$ |
| k_p^R | $k_p^R = k_p / (1 + Rk_p / r_p)$ |
| L | length, m |
| l | mean free path, m |
| m | mass, kg |
| n | distribution function |
| Nu | Nusselt number, $Nu = hD/k$ |
| Pe | Peclet number, $Pe = GDC_p/k$ |
| Pr | Prandtl number, $Pr = C_p\mu/k$ |
| Q | heat, J |
| R | boundary resistance, m^2K/W |
| r | radius, m |
| r_a | aggregate gyration radius, m |
| r_c | cluster gyration radius, m |
| Ra | Rayleigh number, $Ra = g\alpha\Delta TD^3 / (v\kappa)$ |
| Re | Reynolds number, $Re = GD/\mu$ |
| s_p | interparticle spacing, m |
| s_r | relative sediment volume |
| T | temperature, K |
| u | parameter, $0 \leq u < \infty$ |
| V | volume, m^3 |
| v | volume concentration |
| v_{pmax} | maximum particle packing volume concentration |

v_r parameter, $v_r = v_p/v_c$
 x axial distance, m

Greek symbols

α thermal expansion coefficient, 1/K
 β particle motion related parameter
 δ_v^+ dimensionless thickness of the laminar sublayer
 κ thermal diffusivity, m²/s
 μ viscosity, kg/ms
 ν kinematic viscosity, m²/s
 ρ density, kg/m³
 σ standard deviation
 σ_1 k_p/k_m dependent parameter
 σ_p Poisson's ratio
 Ψ sphericity

Subscripts

a aggregation
 b boiling, bulk
 c complex particle
 e effective
 m base fluid matrix
max maximum
 p particle
 s shell
 v laminar sublayer
 w wall

Review and Assessment of Nanofluid Technology for Transportation and Other Applications

Wenhua Yu, David M. France, Stephen U. S Choi, and Jules L. Routbort

Energy Systems Division, Argonne National Laboratory, Argonne, IL 60439, USA

Abstract

This report provides a literature review on the research and development work contributing to the current status of nanofluid technology for heat transfer applications in industrial processes. Nanofluid technology is a relatively new field, and as such, the supporting studies are not extensive. Specifically, the experimental results and theoretical predictions regarding the enhancement of the thermal conductivity and convective heat transfer of nanofluids relative to conventional heat transfer fluids were reviewed and assessments were made of the current status to derive future research and development directions for industrial applications. Pertinent parameters were considered individually as to the current state of knowledge. Experimental results from multiple research groups were cast into a consistent parameter, “the enhancement ratio,” to facilitate comparisons of data among research groups and identification of thermal property and heat transfer trends. The current state of knowledge is presented as well as areas where the data are currently inconclusive or conflicting. Heat transfer enhancement for available nanoparticles is shown to be in the 15-40% range, with a few situations resulting in orders of magnitude enhancement. The direction of future research should be to substantiate the lower range results and to continue investigations into the higher enhancements. The focus of this study is primarily transportation applications. However, some attention is given to other industrial applications of nanofluid heat transfer. Also discussed are barriers to be addressed prior to commercialization of nanofluids.

1. Introduction

Many industrial processes involve the transfer of heat by means of a flowing fluid in either the laminar or turbulent regime as well as flowing or stagnant boiling fluids. The processes cover a large range of temperatures and pressures. Many of these applications would benefit from a decrease in the thermal resistance of the heat transfer fluid. This situation would lead to smaller heat transfer systems with lower capital costs and improved energy efficiencies. Nanofluids have the potential to reduce such thermal resistances, and the industrial groups that would benefit from such improved heat transfer fluids are quite varied. They include transportation, electronics, medical, food, and manufacturing of many types.

“Nanofluid” is the name conceived by Argonne National Laboratory to describe a fluid in which nanometer-sized particles are suspended. Nanofluids consisting of such particles suspended in liquids (typically conventional heat transfer liquids) have been shown to enhance the thermal conductivity and convective heat transfer performance of the base liquids. The thermal conductivities of the particle materials are typically order-of-magnitude higher than those of the base fluids such as water, ethylene glycol, and light oils, and nanofluids, even at low volume concentrations, result in significant increases in thermal performance.

Nanofluids are nanotechnology-based heat transfer fluids that are derived by stably suspending nanometer-sized particles (with typical length scales of 1 to 100 nm) in conventional heat transfer fluids – usually liquids. Research results from nanofluid research groups worldwide show that nanofluids have thermal properties that are very different from those of conventional heat transfer fluids. In one study, the addition of a small amount (less than 1 percent by volume) of nanoparticles to conventional heat transfer liquids increased the thermal conductivity of the fluids up to approximately two times (Choi, et al. 2001). As will be discussed subsequently, many researchers have determined the thermal conductivity enhancement of different nanoparticles in a variety of liquids with volume concentrations to be in the range of 0.5-4%. At these low particle volume concentrations, typical enhancement has been in the 25% range over the base fluid. The distinctive features of nanofluids include a stronger temperature-dependent thermal conductivity than in the base fluid alone (Das, et al. 2003a), a substantial increase in thermal conductivity with low particle volume concentrations (Choi, et al. 2001), an increase in critical heat flux (CHF) in pool boiling (You, et al. 2003), and a substantial increase in the heat transfer coefficient at low particle volume concentrations. The heat transfer coefficient is the determining parameter in forced-convection cooling applications, including engines and engine systems. More important, experiments have shown that nanoparticles significantly enhance the heat transfer coefficients of flowing liquids, and some experimenters have claimed substantial enhancements (Faulkner, et al. 2004). This topic will be discussed in detail subsequently, where results from multiple experimenters will be presented and compared. At this point, it is notable that many of the higher levels of heat transfer coefficient enhancement reported are beyond the effect of increased thermal conductivity alone. Thus, the potential impact of nanofluids on general heat transfer applications is quite large, and this includes ethylene glycol and water mixtures for engine cooling.

In addition to the numerous experimental investigations into nanofluid thermal properties and heat transfer, various investigators have proposed physical mechanisms and mathematical models to describe and predict the phenomena. While comprehensive theoretical models for nanofluids that take all main factors into account are lacking, some progress has been made in this area. Consequently, the classical models and new improvements are presented in this study.

2. Nanofluid Research

Argonne National Laboratory was a pioneer in the early days of research and development of nanofluid technology. Initial demonstrations of the excellent potential of nanofluids for heat transfer applications led both industry and universities to launch research and development efforts in nanofluid technology. That effort has increased considerably over the past several years, as is evident from the compilation of yearly publications shown in Figure 1.

More than 250 nanofluid-related research publications have appeared since 1995, and the number per year should continue to increase. Of these, Argonne National Laboratory has produced more than 30 in peer-reviewed publications. In 2006 alone, more than 100 research papers were published in *Science Citation Index* journals. Some of this publication increase is due to the establishment of nanofluid research groups at prestigious institutions worldwide. Research is also coming from small businesses and large multinational companies in different industries and markets for specific applications. Much of this escalating interest in nanofluids is based on the potential for high-performance coolants. For the automotive industry, the fluids of interest are liquids at low pressure and engine operating temperatures. Ethylene glycol (or ethylene glycol and water mixtures) is the most desirable base fluid for cooling systems for historical reasons. Nanofluids with engine oils as base fluids have automotive applications as well. However, the transition to industrial practice requires that nanofluid technology become further developed and that some key barriers be overcome.

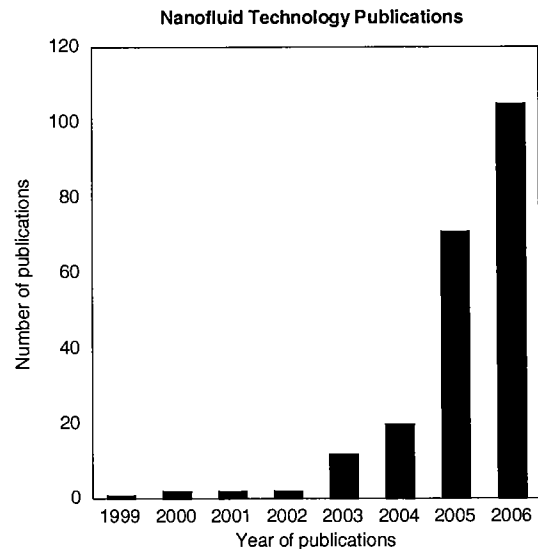


Figure 1. Nanofluid technology publication rate

3. Production of Nanoparticles and Nanofluids

Modern fabrication technology allows the fabrication of materials at the nanometer scale. Nanoparticles are a class of materials that exhibit unique physical and chemical properties compared to those of larger (micron scale and larger) particles of the same material. Nanoparticles used in nanofluids have been made out of many materials, and the fabrication of nanoparticles can be classified into two broad categories: physical processes and chemical processes.

Some nanoparticle materials that have been used in nanofluids are oxide ceramics (Al_2O_3 , CuO), nitride ceramics (AlN , SiN), carbide ceramics (SiC , TiC), metals (Ag , Au , Cu , Fe), semiconductors (TiO_2), single-, double- or multi-walled carbon nanotubes (SWCNT, DWCNT, MWCNT), and composite materials such as nanoparticle core-polymer shell composites. In addition, new materials and structures are attractive for use in nanofluids where the particle-liquid interface is doped with various molecules.

Nanoparticles of various materials have been produced by physical or chemical synthesis techniques. Typical physical methods include the mechanical grinding method and the inert-gas-condensation technique. The later was developed by Granqvist and Buhrman of Cornell University (Granqvist and Buhrman 1976). Chemical methods for producing nanoparticles include chemical precipitation, chemical vapor deposition, micro-emulsions, spray pyrolysis, and thermal spraying. Also, a sonochemical method has been developed to make suspensions of iron nanoparticles stabilized by oleic acid (Kenneth, et al. 1996). Current processes specifically for making metal nanoparticles include mechanical milling, inert-gas-condensation technique, chemical precipitation, spray pyrolysis, and thermal spraying.

Nanoparticles in most materials discussed are most commonly produced in the form of powders. In powder form, nanoparticles can be dispersed in aqueous or organic host liquids to form nanofluids for specific applications. To date, many types of host liquids have been used, but ethylene glycol or ethylene glycol and water mixtures are the most desirable for automotive applications. Several materials for the nanoparticles seem to have good potential for such applications.

Nanofluids have been produced by two techniques: the two-step technique and the single-step technique. The two-step technique starts with nanoparticles, produced by one of the physical or chemical synthesis techniques described previously, and proceeds to disperse them into a base fluid. The single-step simultaneously makes and disperses the nanoparticles directly into a base fluid. Most of the nanofluids containing oxide nanoparticles and carbon nanotubes reported in the open literature are produced by the two-step process.

4. Barriers and Challenges to the Commercial Production of Nanofluids

To date, nanofluids of various qualities have been produced mainly in small volumes. This production has been adequate for research work, but large-scale production of well-dispersed nanofluids at low cost is required for commercial applications. This production situation is a serious barrier to testing and use of nanofluids in the radiator coolant systems of vehicles and other vehicle oils.

4.1. Two-Step Process

An advantage of the two-step technique in terms of eventual commercialization of nanofluids is that Nanophase Technologies Corporation has already scaled up the inert gas condensation technique to economically produce tonnage quantities of nanoparticles (Romano, et al. 1997). Such nanopowders produced economically in bulk can be used to make nanofluids by the two-step method if the agglomeration problem can be overcome. Making nanofluids using the two-step processes was and remains a challenge because individual particles tend to quickly agglomerate before complete dispersion can be achieved. This agglomeration is due to attractive van der Waals forces between nanoparticles, and agglomerations of particles tend to quickly settle out of liquids. In fact, agglomeration is a critical issue in all nanopowder technology, including nanofluid technology, and a key step to success in achieving high-performing heat transfer nanofluids is to produce and suspend nearly monodispersed or non-agglomerated nanoparticles in liquids. This barrier is exacerbated by the use of oxide nanoparticles that require higher volume concentrations compared to metal particles to achieve the same heat transfer enhancement in nanofluids. At high volume concentrations, the agglomeration problem becomes worse. Some surface-treated nanoparticles show excellent dispersion in base fluids and good thermal properties. The challenge is to develop innovative ways to improve the two-step process to produce well-dispersed nanofluids in large volumes. Some fluids are currently available commercially in the form of liquid suspensions of small particles. Ceramic suspensions are available in large quantities. Magnetic fluids containing iron oxide particles have been available in the market since the 1970s. These fluids exhibit the same agglomeration and settling problems as nanofluids made in laboratory environments by the two-step process.

4.2. One-Step Process

For nanofluids containing high-conductivity metals such as copper, a single-step technique is preferable to the two-step process to prevent oxidation of the particles. With this technique, nanoparticles are formed and dispersed in a fluid in a single process. Argonne National Laboratory developed a one-step physical method for creating nanofluids. This patented single-step method involves direct evaporation and has been used to produce non-agglomerating copper nanoparticles that remain uniformly dispersed and stably suspended in ethylene glycol. This technique involves condensing nanophase powders from the vapor phase directly into a flowing low-vapor-pressure ethylene glycol in a vacuum chamber. The well-dispersed nanofluids of Cu in ethylene glycol enhance the thermal conductivity of the base fluid by up to 40% at the particle volume concentration of 0.3 vol. %, significantly larger than the prediction of effective medium theory (Eastman, et al. 2001). Another one-step physical method, submerged arc nanoparticle synthesis, has been reported as being used to produce nanofluids containing various

nanoparticles such as TiO₂, CuO, and Cu (Chang, et al. 2005; Lo, et al. 2005a; Lo, et al. 2005b). With this method, the nanoparticles are produced by heating the solid material from an electrode by means of arc sparking and then condensing it into liquid in a vacuum chamber to form a nanofluid.

Although the one-step physical methods have produced nanofluids in small quantities for research purposes, they are unlikely to become the mainstay of commercial nanofluid production. They would be difficult to scale up for two reasons. Processes that require a vacuum significantly slow the production of nanoparticles and nanofluids, thus limiting the rate of production. Furthermore, producing nanofluids by these one-step physical processes is expensive.

Recently, an alternative one-step chemical method for making copper nanofluids has been reported (Zhu, et al. 2004). Nearly monodispersed copper nanoparticles with less than 20-nm diameter were reportedly produced and dispersed in ethylene glycol by the reduction of a copper salt by sodium hypophosphite. Polyvinylpyrrolidone was added as a protective polymer and stabilizer that inhibited particle agglomeration. Copper nanofluids produced by this one-step chemical method show nearly the same thermal conductivity enhancement as the nanofluids produced by the one-step physical method. More recently, Argonne has successfully made small amounts of nanofluids by this process. With some development, this method has the potential to produce large quantities of nanofluids faster than the one-step physical process. However, a significant limitation to this technique is that the volume concentration of nanoparticles and quantities of nanofluids that can be produced are much limited than those of the two-step technique.

Unlike the two-step process, these one-step processes are not commercially available yet. A major challenge is to develop innovative ways to improve the one-step chemical process to economically produce large quantities of nanofluids.

A drawback to both physical and chemical one-step processes for nanofluid production is that systems run in batch mode with limited control over a number of important parameters, including those that control nanoparticle size. Being able to run the one-step chemical process in a continuous mode would increase its commercial viability. To that end, McGill University has recently developed a semi-continuous process for the one-step production of ethylene glycol-based nanofluids containing copper nanoparticles coated with an ultrathin (2-10 nm) organic layer, which is chemically compatible with the host fluid and thereby ensures the stabilization of the suspension (Cao and Tavares 2006).

4.3. Other Processes

While most nanofluid productions to date have used one of the above-described (one-step or two-step) techniques, other techniques are available depending on the particular combination of nanoparticle material and fluid. For example, nanoparticles with specific geometries, densities, porosities, charge, and surface chemistries can be fabricated by templating, electrolysis metal deposition, layer-by-layer assembly, microdroplet drying, and other colloid chemistry techniques. Another process, the chemical vapor condensation technique, appears to offer

advantages in terms of control of particle size, ease of scalability, and the possibility of producing novel core-shell nanostructures (Srđić, et al. 2001). Still another technique is the shape- and size-controlled synthesis of nanoparticles at room temperature (Cao, et al. 2006). The structural characteristics of nanoparticles such as the mean particle size, particle size distribution, and shape depend on the synthesis method, and there is potential for good control. These characteristics for nanoparticles in suspensions are not easily measured. This fact could account for some of the discrepancies in thermal properties reported in the literature among different experimenters. Such discrepancies will be discussed subsequently.

5. Experimental Research on Nanofluid Thermal Conductivity

The heat transfer resistance of a flowing fluid is often represented by a Nusselt number, which takes into account the fluid thermal conductivity directly and usually indirectly as well through the Prandtl number. Thus, a first assessment of the heat transfer potential of a nanofluid is to consider its thermal conductivity. To date, more research has been published in this area than in any other related to nanofluids for heat transfer purposes, and many of these studies have focused on automotive applications.

In examining the engineering literature, we have gathered experimental data from many researchers. In each case, the thermal conductivity enhancement ratio has been calculated from the information given in the technical papers. The thermal conductivity enhancement ratio, or simply the “enhancement,” is defined as the ratio of the thermal conductivity of the nanofluid to the thermal conductivity of the base fluid. The percent enhancement in thermal conductivity is the enhancement ratio, minus one, times 100%. For consistency in this study, the term “enhancement” refers to the enhancement ratio with regard to any parameter such as thermal conductivity, heat transfer coefficient, and Nusselt number. When a percentage enhancement is given, it will be so noted.

Table 1 of Appendix A provides a compilation of the data collected for the thermal conductivity of nanofluids from experiments. The first column gives the name of the lead author and the date of each paper. The “nanofluid” column gives the combinations of particle material and base fluid used along with the temperature. The “concentration” column gives the range of particle volume concentrations tested. The “particle size” is given as the average diameter of spherical particles unless another particle shape is noted. In almost all nanofluid studies, the particle size distribution is unknown. Even if the distribution is known for the particles in powder form, for the two-step nanofluid production method, the effects of particle agglomeration or settling out of suspension are usually unknown. (Production method is given in the “note” column in Table 1, and particle agglomeration and settling out of suspension need to be minimized in commercial nanofluids to be discussed subsequently.) Note that at the experimental level, the mean particle size in the fluid can differ from the powder size, and particle size distribution can be different among experimenters reporting the same mean size. Finally, the results of the experiments in terms of the thermal conductivity enhancement ratio are given in Table 1 as calculated from the information given in the papers.

The eight parametric effects on nanofluid thermal conductivity enhancement, isolated from among the experimental data of Table 1, are (1) particle volume concentration, (2) particle material, (3) particle size, (4) particle shape, (5) base fluid material, (6) temperature, (7) additive, and (8) acidity. Each of these eight parameters will be considered separately from the standpoint of data trend, magnitude, and corroboration by multiple experimenters.

5.1. Effect of Particle Volume Concentration

The effect of particle volume concentration on nanofluid thermal conductivity enhancement is shown in Figure 2, where the works of seven experimental groups are presented for Al_2O_3 in water. The particle size and nanofluid temperature vary among groups in Figure 2, but the

general trend is clear: thermal conductivity enhancement increases with increased particle volume concentration. Oxide-particle volume concentrations are normally below 4 to 5% to maintain moderate viscosity increases, and an enhancement level up to about 1.3 (30%) is typical.

The effect of particle volume concentration on thermal conductivity enhancement is isolated in Figure 3 by comparing the data of two research groups using the same nominal size particles. Considering the available information, the two groups of Figure 3 used the same parameters, and the results are nearly identical. (The magnitude of the enhancement in Figure 3 is relatively low due to the rather small particle diameter.) The same trends were observed with other particle and fluid combinations and other particle sizes.

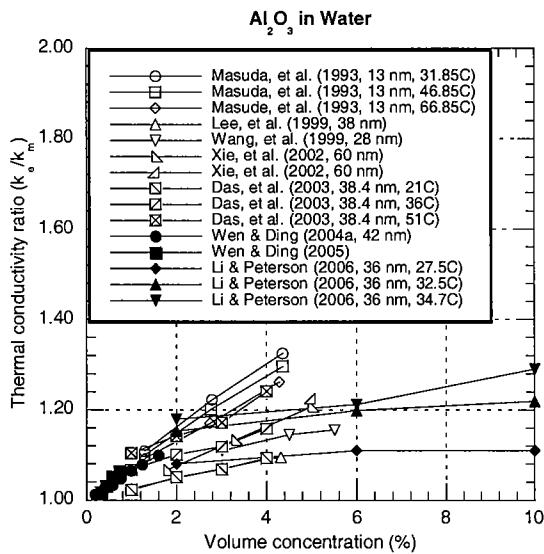


Figure 2. Thermal conductivity enhancement of Al₂O₃ in water

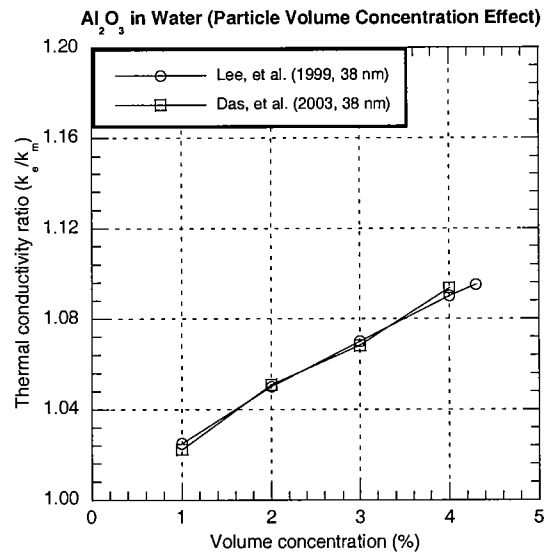


Figure 3. Effect of particle volume concentration for Al₂O₃ in water

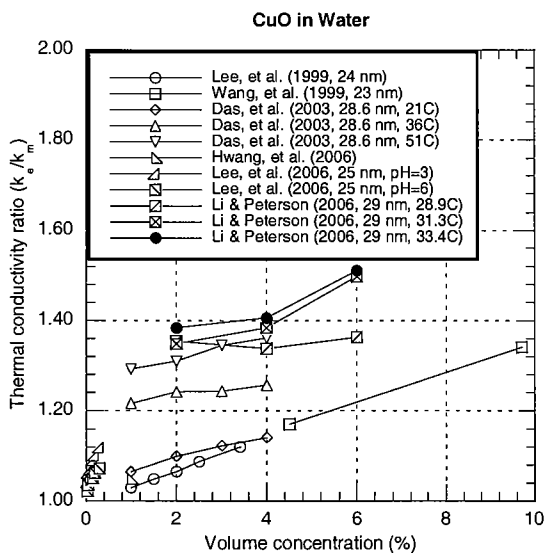


Figure 4. Thermal conductivity enhancement of CuO in water

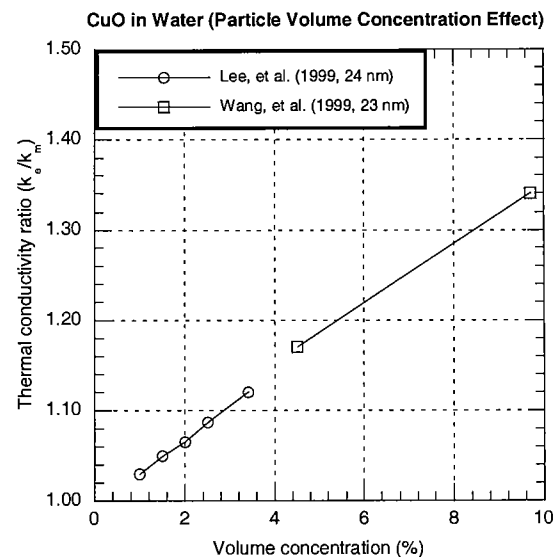


Figure 5. Effect of particle volume concentration for CuO in water

Results from several experimenters for thermal conductivity enhancement are shown in Figure 4 for CuO in water. As in Figure 2, a range of particle sizes and fluid temperatures is included in Figure 4. The volume concentration parameter is isolated for CuO in Figure 5, where one particle size and one fluid temperature are used. The general trend is the same in Figures 2-5, and magnitudes are corroborated in Figures 3 and 5 by two groups of experimenters in each.

The effect of particle volume concentration with ethylene glycol as the base fluid is seen in Figure 6 to have the same trend as the water data of Figures 2-5. The agreement in magnitude is good between the data of the two research groups of Figure 6. From Figures 2-6, it is clear that the general trend is for increased thermal conductivity enhancement with increased particle volume concentration. Several studies are included in the comparisons, and experimental groups agreed on magnitude of enhancement with reportedly identical test parameters for Al₂O₃ in water (Lee, et al. 1999 and Das, et al. 2003), CuO in water (Lee, et al. 1999 and Wang, et al. 1999), and CuO in ethylene glycol (Lee, et al. 1999 and Wang, et al. 1999). At higher particle volume concentrations, the increase in enhancement is expected to diminish or even reverse. Also, nanofluid viscosity would increase. However, in the practical volume concentration range for automotive applications shown in the figures, no results were found in the literature that contradicted the upward trend. The same is not true for the other seven parameters to be presented next.

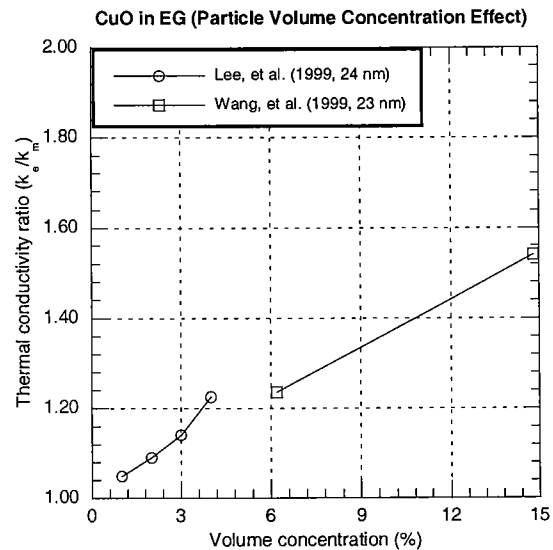


Figure 6. Effect of particle volume concentration for CuO in ethylene glycol

5.2. Effect of Particle Material

The effect of particle material on thermal conductivity enhancement is shown in Figure 7 for two oxide particles and silicon carbide – all in water. All other parameters are approximately constant in Figure 7, isolating the material property effect. As shown, the particle material has essentially no effect on the enhancement for these relatively low thermal conductivity particles. The situation changes when higher conductivity particles are used, as presented next.

The results for thermal conductivity enhancement shown in Figure 8 include two metal particles and one oxide for comparison. As shown, the metal particles produce the same enhancement as the oxide particles but at much lower volume concentration. It was expected that metal particles would outperform oxide particles owing to the higher thermal conductivity of the former. It is difficult to create metal particle nanofluids without the particles oxidizing during the production process. The Cu particles of Figure 8 were produced by the one-step method.

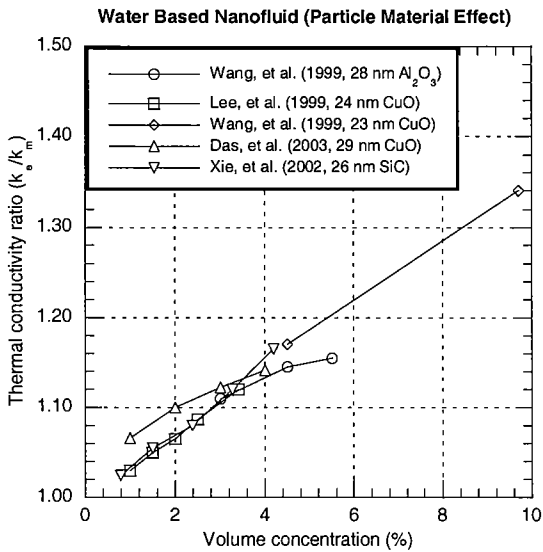


Figure 7. Effect of particle material for particles in water

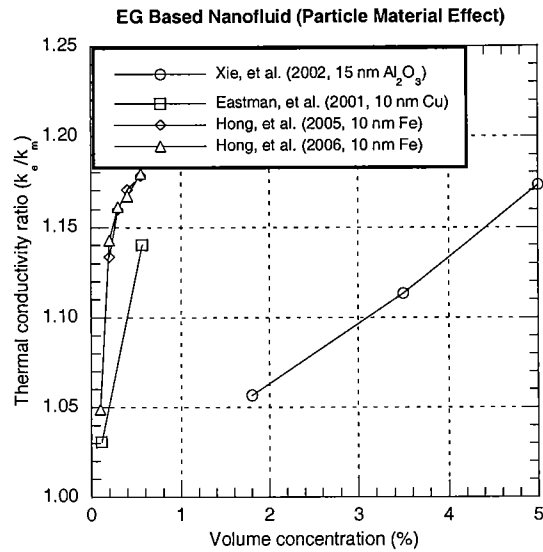


Figure 8. Effect of particle material for particles in ethylene glycol

In Figure 8, the thermal conductivity ratio is seen to increase faster for metal than oxide particles. One wonders how high the ratio could go had the metal particle experiments been carried out to higher volume concentration levels. Part of the answer is seen in Figure 9. Here results are presented for oxide, silicon carbide, and metal particles. The particles in Figure 9 are larger in size than in Figure 8, but the main effect shown is the very high thermal conductivity enhancement of the metal-particle nanofluid when the particle volume concentration was increased to 2.5% compared to the maximum of about 0.7% for the metal particles of Figure 8. At a metal particle volume concentration of 2.5%, the thermal conductivity of the nanofluid is seen in Figure 9 to be 115% above ethylene glycol. This result is significantly higher than the non-metallic particle results of Figure 9 and points to a direction for nanofluid research and production. However, as mentioned previously, a major obstacle for metal-particle nanofluids is eliminating the oxidation process during production and later during usage. Particle coating is one technique that has received some attention to solve this problem.

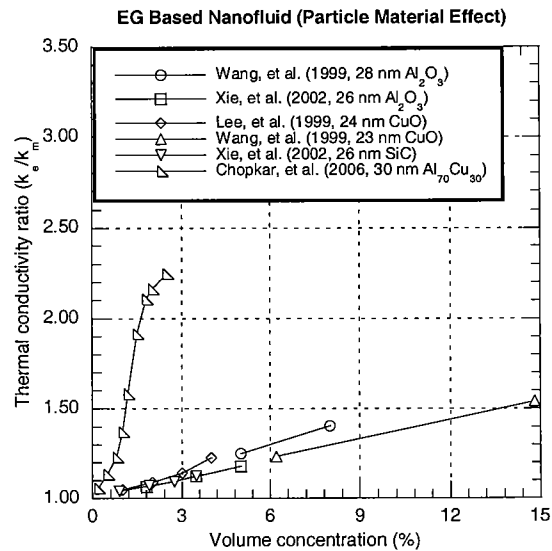


Figure 9. Effect of particle material for particles in ethylene glycol

5.3. Effect of Particle Size

The effect of particle size on thermal conductivity enhancement was considered next. Only particles reported to be spherical were included, with the size parameter being the nominal diameter. Results are shown in Figure 10 for a single particle/water combination over a range of

particle diameter from 28 to 60 nm. The trends shown are not monotonic. There is agreement between two research groups studying of 38-nm particles. The results for larger particles, 60 nm, show an increase in thermal conductivity enhancement. Based on these results, one would expect that the smallest particles would show the least enhancement. However, the results for the 28-nm particles fall between the two larger sizes. The range in particle size is relatively small in Figure 10, for which data are available with all other parameters the same. The results of Figure 10 are not conclusive with respect to trend. The same is true for the results for a limited particle size range in ethylene glycol, shown in Figure 11. Here, the thermal conductivity enhancement is largest for the intermediate-sized particle.

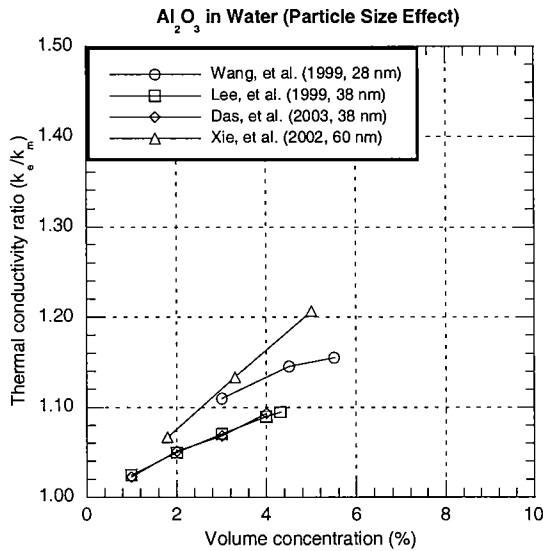


Figure 10. Effect of particle size for Al₂O₃ in water

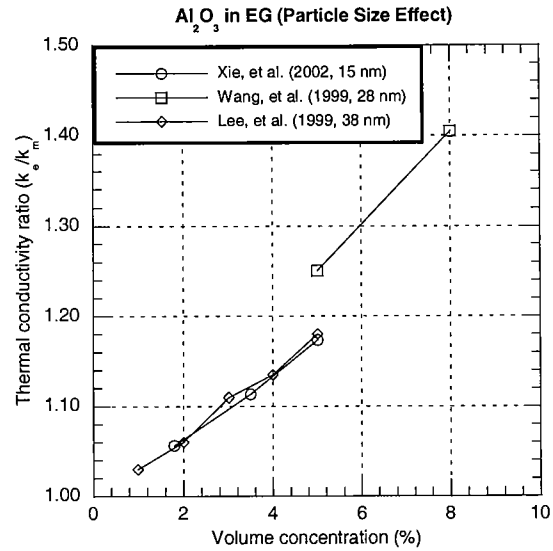


Figure 11. Effect of particle size for Al₂O₃ in ethylene glycol

From the trends of Figures 10 and 11, we concluded that, omitting the data of Wang et al. (1999), a consistent trend appears wherein the larger particle diameters produce a large enhancement in thermal conductivity. This result is in disagreement with some theories that point to a uniform distribution of small particles as producing the best enhancement. With particle agglomeration being a key but largely unknown factor in most thermal conductivity experiments, the particle size effect from experiment and theory may not actually be on the same basis. It should be emphasized that in this case, as in all nanofluid data comparisons of this study, uncertainty arises from the accuracy of the reported particle size and shape. These parameters are most often not measured by the experimenters but rather taken from the powder manufacturers' nominal information.

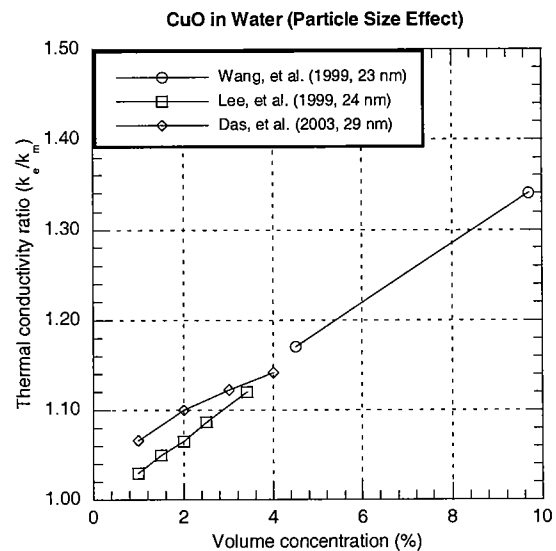


Figure 12. Effect of particle size for CuO in water

A third comparison of particle size effect on

thermal conductivity enhancement is shown in Figure 12 for CuO in water. Here, the results of Wang et al. (1999) are separated from the other two groups whose results show the trend of increase enhancement with increased particle size. The results of Figures 10-12 suggest that the thermal conductivity enhancement increases with the diameter of the suspended spherical nanometer particles.

5.4. Effect of Particle Shape

Thermal conductivity enhancement in nanofluids was compared with respect to the geometric shape of the particles. In Figure 13, spherical and cylindrical particle shapes are compared. The cylinders show an increase in thermal conductivity enhancement, and this result is thought to be due to a mesh formed by the elongated particles that conducts heat through the fluid. The results of Figure 13 are from a single group, and that is the case with the remainder of the available data shown in Figures 14 and 15. However, all of the results of Figures 13-15 indicate that elongated particles are superior to spherical for thermal conductivity enhancement. This result points to a direction for nanofluid research and production although spherical particles are often most readily available at the best prices.

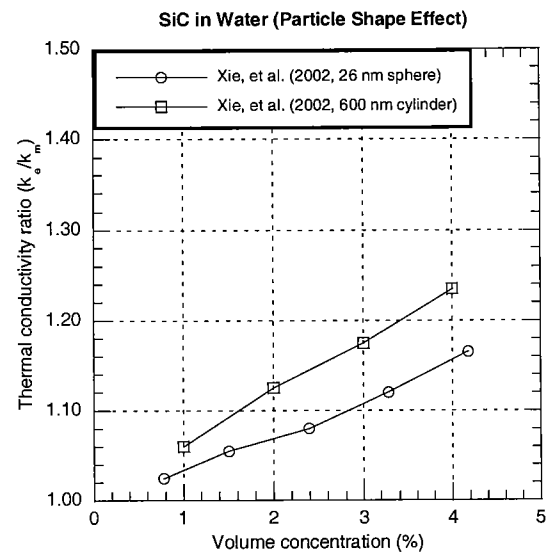


Figure 13. Effect of particle shape for SiC in water

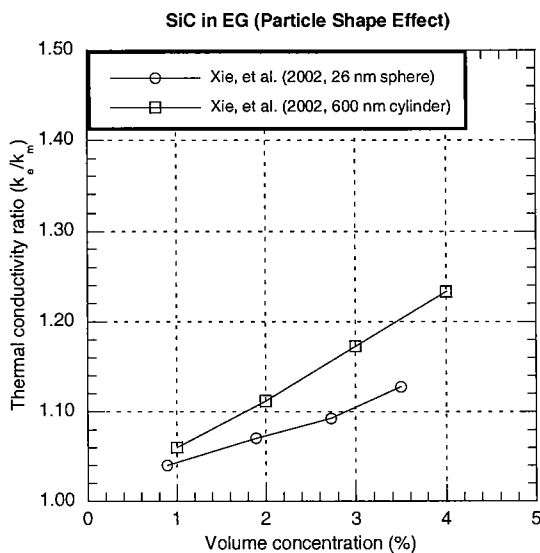


Figure 14. Effect of particle shape for SiC in ethylene glycol

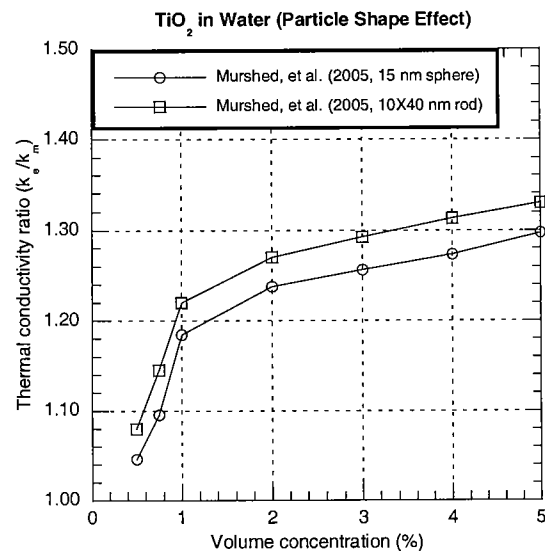


Figure 15. Effect of particle shape for TiO₂ in water

5.5. Effect of Base Fluid Material

The influence of base fluid itself (such as water, ethylene glycol, and pump oil) on the enhancement in thermal conductivity of nanofluids is shown in Figure 16. The results show increased thermal conductivity enhancement for poorer (lower thermal conductivity) heat transfer fluids. The results of Figure 16 show the least enhancement for water, which is the best heat transfer fluid with the highest thermal conductivity of the fluids compared. Although this trend was not supported in all cases for the experimental data reviewed, it was generally the case. This result is encouraging because heat transfer enhancement is often most needed when poorer heat transfer fluids are involved. Ethylene glycol alone is a relatively poor heat transfer fluid compared with water, and mixtures of ethylene glycol and water fall between the two in heat transfer effectiveness. Thus, nanoparticles in ethylene glycol and water mixtures show good potential for engine cooling applications.

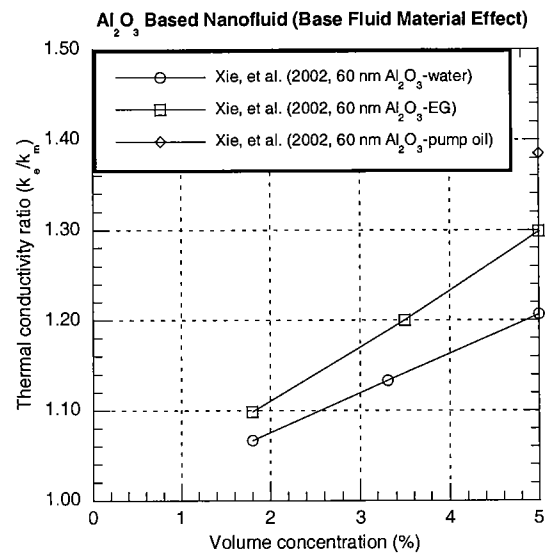


Figure 16. Effect of base fluid material for Al₂O₃ in fluids

5.6. Effect of Temperature

In general, the thermal conductivity of nanofluids is more temperature sensitive than that of the base fluid. Consequently, the thermal conductivity enhancement of nanofluids is also rather temperature sensitive. In each of the data comparisons that follow, results are plotted for one research group at a time. This situation arises mainly from the diverse values of temperatures used by the experimenters. Although there are no direct comparisons of data among experimenters, the trends of all but one experimental group show increased thermal conductivity enhancement with increased temperature. Das et al. (2003) presented nanofluid data over a small temperature range for Al₂O₃ in water and for CuO in water. They suggested that the rather strong temperature dependence of nanofluid thermal conductivity is due to the motion of nanoparticles.

Results for Al₂O₃ in water are shown in Figures 17-19 for three groups. Particle sizes and fluid temperatures differ among the figures, but particle size is constant in each figure and temperature varies in each. Only the results of Masuda et al. (1993) disagree with the general trend.

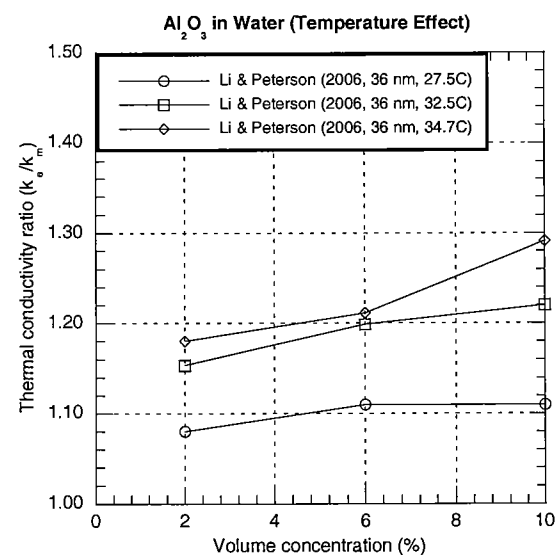


Figure 17. Effect of temperature for Al₂O₃ in water

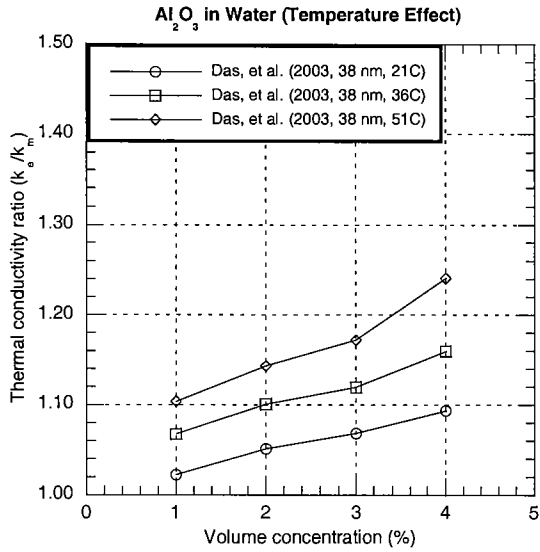


Figure 18. Effect of temperature for Al₂O₃ in water

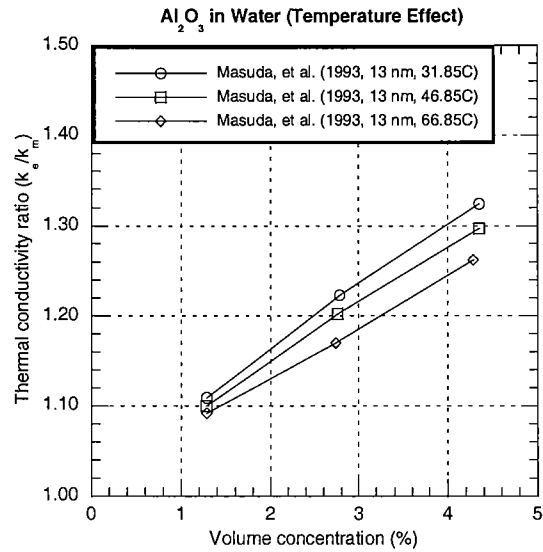


Figure 19. Effect of temperature for Al₂O₃ in water

Thermal conductivity enhancement for CuO in water is shown in Figures 20 and 21 for two research groups. The data clearly follow the general temperature trend where enhancement increases with increased temperature. As shown in Figures 22 and 23, similar results were obtained from two sets of experiments for MWCNT in water.

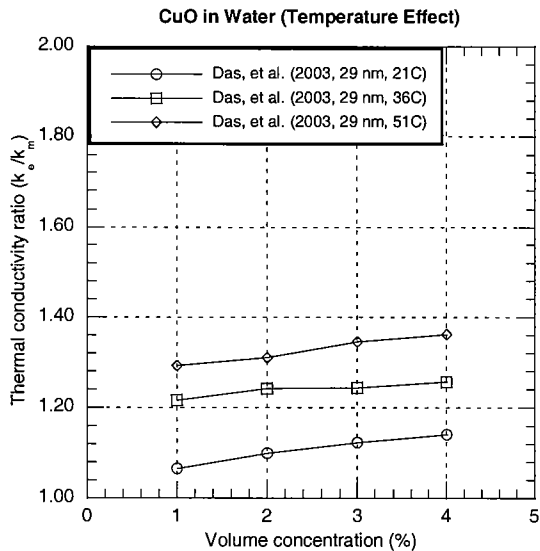


Figure 20. Effect of temperature for CuO in water

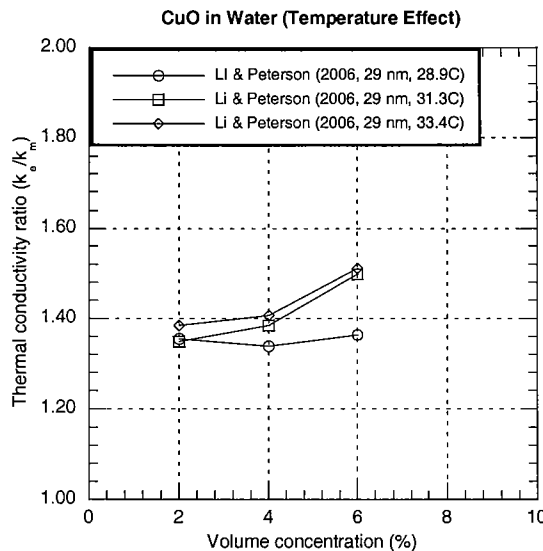


Figure 21. Effect of temperature for CuO in water

It should be noted that the one set of data that is not consistent with the general temperature trend is in itself not completely consistent. The opposite temperature trend was report by Masuda et al. (1993) for SiO₂ in water, but for TiO₂ in water the results were not monotonic with respect to temperature. All results considered, we find substantial support for the general temperature

trend presented. This trend is encouraging for engine and heat exchanger applications in the transportation industry, where fluids operate at elevated temperatures.

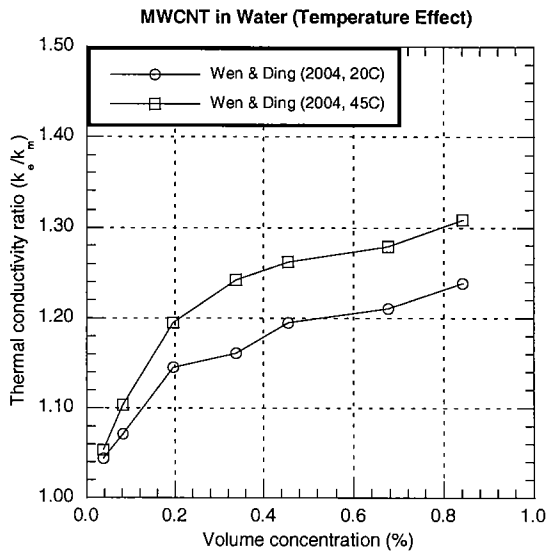


Figure 22. Effect of temperature for MWCNT in water

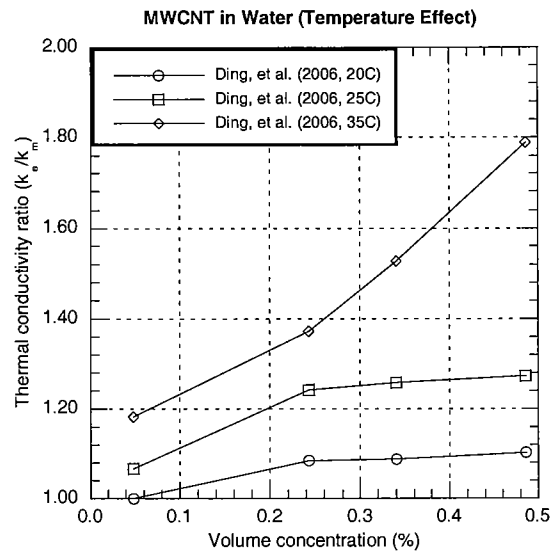


Figure 23. Effect of temperature for MWCNT in water

5.7. Effect of Additives

Experimenters have used fluid additives in an attempt to keep nanoparticles in suspension and to prevent them from agglomerating. The results in the literature are scattered and wide-ranging with respect to additive type, concentration, etc. However, most studies involving additives show enhancement in the thermal conductivity ratio as a result. The data from two such studies are presented in Figures 24 and 25 for different nanofluids and additives. In both cases, the thermal conductivity enhancement improved by using the additive. Here again there is direction for future research and production development. At the present time, few studies have been published on this subject, making it a new and potentially rewarding area to pursue.

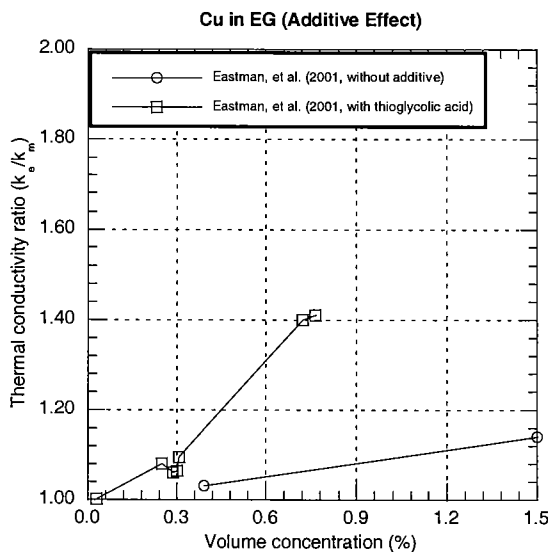


Figure 24. Effect of additive for Cu in ethylene glycol

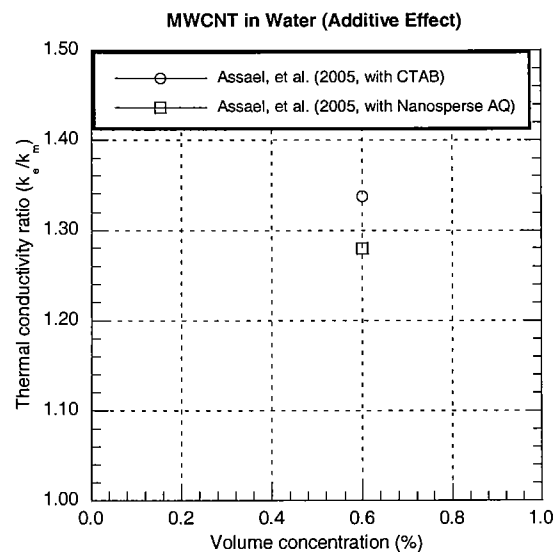


Figure 25. Effect of additive for MWCNT in water

5.8. Effect of Acidity (pH)

Limited studies have been published on the effect of fluid acidity on the thermal conductivity enhancement of nanofluids. The results from two groups are presented separately below. The results of Figures 26 and 27 for different particles in water exhibit the same trend. The finding that acidity increases the thermal conductivity enhancement has not been explained.

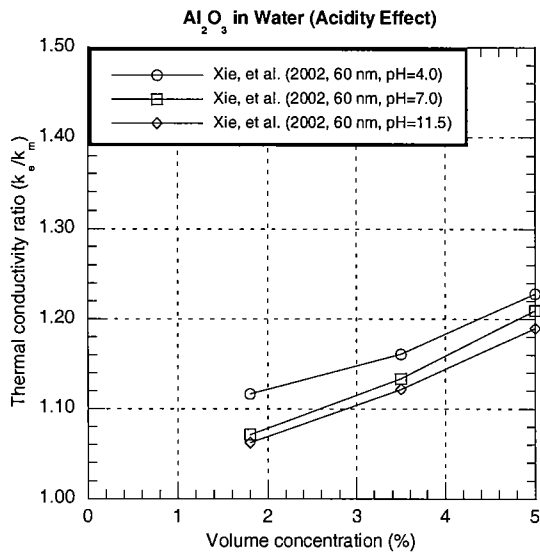


Figure 26. Effect of acidity for Al₂O₃ in water

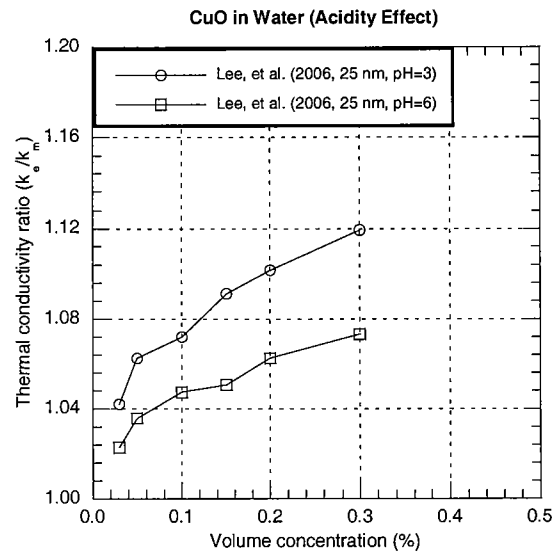


Figure 27. Effect of acidity for CuO in water

6. Experimental Research on Heat Transfer

While increases in effective thermal conductivity as well as changes in density, specific heat, and viscosity are important indications of improved heat transfer behavior of nanofluids, the net benefit of nanofluids as heat transfer fluids is best determined through the heat transfer coefficient. If nanofluids can improve the heat transfer coefficient of vehicle and other thermal energy systems, they can facilitate the reduction in size of such systems and lead to increased energy and fuel efficiencies, lower pollution, and improved reliability. To this end, it is essential to directly measure the heat transfer performance of nanofluids under flow conditions typical of specific applications. To date, there has been limited research reported in this area. A summary of that body of work follows.

We have divided the nanofluid heat transfer research by fluid conditions of laminar flow, turbulent flow, and pool boiling. The number of studies in these areas is small, with the least number of studies having been reported in the boiling situation.

6.1. Heat Transfer Enhancement in Laminar Flow

Experimental results on laminar and turbulent flow for nanofluids as reported in the engineering literature are listed in Table 2 of Appendix A. The nanofluid types and testing parameters are listed in the table along with the heat-transfer enhancement ratio determined experimentally. (As part of this study, results from all literature sources were put into the enhancement ratio form for comparison purposes.) The Reynolds number range of each set of experiments is listed in the “note” column.

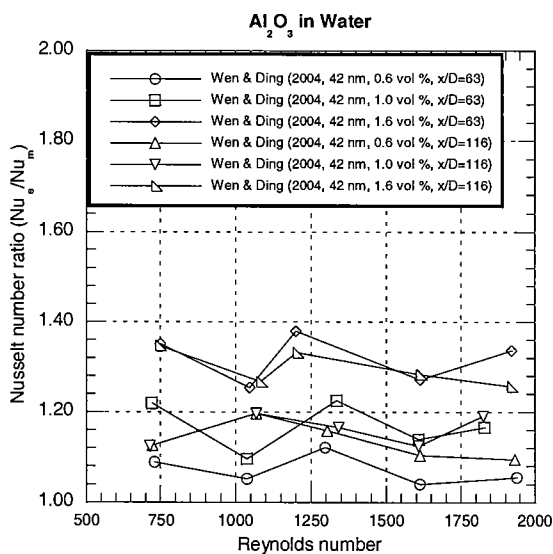


Figure 28. Laminar flow heat transfer of Al₂O₃ in water

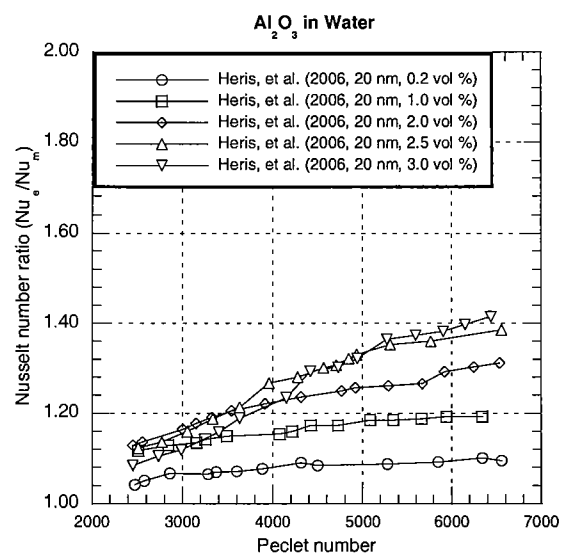


Figure 29. Laminar flow heat transfer of Al₂O₃ in water

Results are shown in Figure 28 for Al₂O₃ in water under laminar flow up to the transition to turbulence. The heat transfer enhancement increases with increasing particle volume concentration as does the thermal conductivity (discussed previously). The heat transfer enhancement is as high as 40% in Figure 28, while the thermal conductivity enhancement was

below 15%. The finding of the heat transfer enhancement exceeding the thermal conductivity enhancement is typical of results reported by some experimenters. This finding indicates that the presence of nanoparticles in the flow influences the heat transfer beyond what would be expected from increased thermal conductivity alone. Some authors have attributed this added effect to particle-fluid interactions. The results of Figure 28 show no influence of heat transfer enhancement due to Reynolds number in this laminar flow region of high Reynolds number.

Similar experiments to those of Figure 28 for alumina in water are shown in Figure 29 from a different group. At particle volume concentrations below 2%, the heat transfer enhancement is comparable between the two groups (Figures 28 and 29), with the enhancement rising even higher in Figure 29 as particle volume concentration increases above 2%. This trend is consistent with the increase of thermal conductivity with increased particle volume concentration, and again the heat transfer enhancement is larger than the thermal conductivity enhancement. The results for the lower particle volume concentrations shown in Figure 29, which are in the same range as in Figure 28, agree with the results of Figure 28, showing little Reynolds number effect on heat transfer enhancement. However, at volume concentrations above 2%, an increase in Reynolds number is seen in Figure 29 to have a positive effect on heat transfer enhancement.

Figures 29 and 30 show heat transfer enhancement for laminar flow with different particle types (Al_2O_3 and CuO) and sizes (20 and 55 nm). The particle volume concentrations are in the same range in the two figures, and the enhancement ratios are as well. These results indicate that particle size and oxide type have minor influence on heat transfer enhancement, which is as high as 40%. More data from other experimenters are required to fully substantiate these results.

Nanofluid heat transfer results for MWCNT in water (Figure 31) show very high heat transfer enhancement, as does the thermal conductivity enhancement as discussed earlier. In this range of intermediate laminar flow Reynolds number, heat transfer rises rapidly at the highest values of Reynolds number. Also

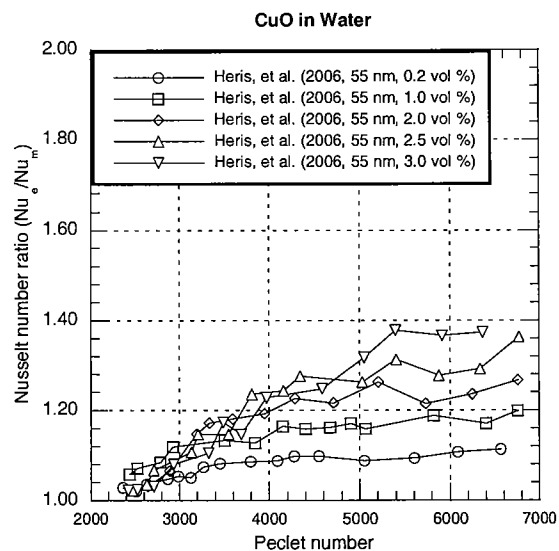


Figure 30. Laminar flow heat transfer of CuO in water

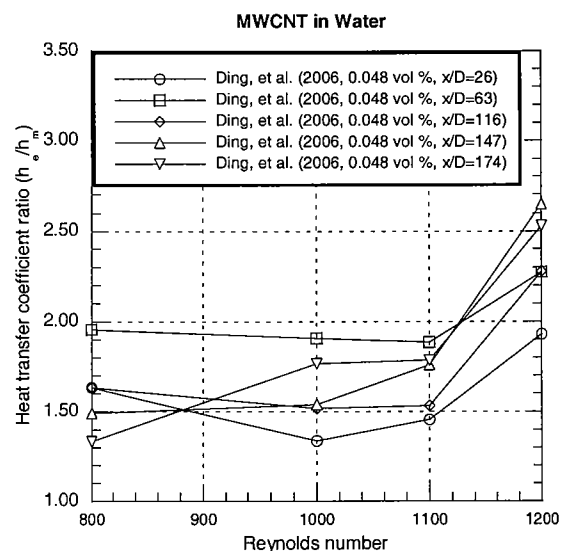


Figure 31. Laminar flow heat transfer of MWCNT in water

shown in Figure 31 is the increased heat transfer enhancement as the flow proceeds downstream at larger axial distance/pipe diameter (x/D).

Results from another experimental group for MWCNT in water with the surfactant sodium dodecylbenzene sulfonate (NaDDBS) are shown in Figure 32. With the exception of one data point in Figure 32, the heat transfer enhancement of up to 2.5 is in agreement with the results of Figure 31. However, there are some striking differences between the parameters of the tests in these two figures. The tests of Figure 32 were run at extremely high nanotube volume concentrations and (perhaps consequently) at very low Reynolds number. Although the general level of heat transfer enhancement agrees with the results of Figure 31, the data of Figure 32 show the opposite trend for heat transfer enhancement as a function of particle volume concentration compared with most other experimenters. From these results, it appears that further substantiation of trends and magnitudes is required at very low flow conditions.

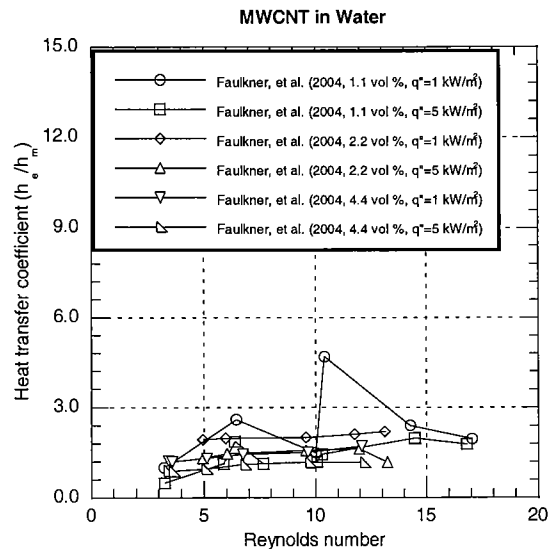


Figure 32. Laminar flow heat transfer of MWCNT in water with NaDDBS

Limited results on nanofluid heat transfer enhancement are available for other base fluids in laminar flow situations. The results of Figure 33 for graphite particles in automotive transmission fluid show no enhancement at low particle volume concentrations, increasing to 25% at a volume concentration of approximately 1%. In synthetic oil mixtures, the trends are much the same as seen in Figure 34, where nanofluids made from different sources of graphite particles were used.

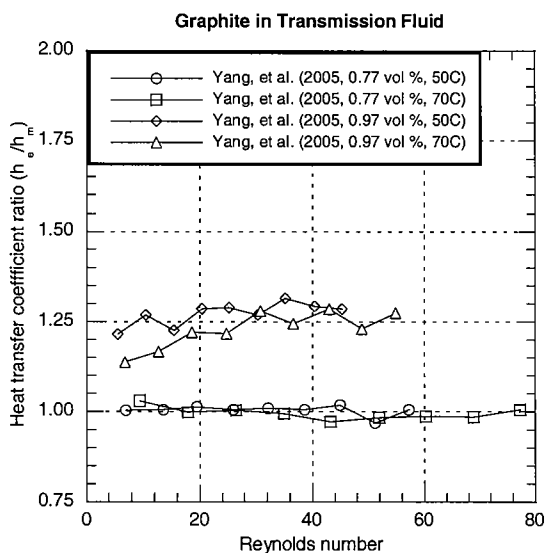


Figure 33. Laminar flow heat transfer of graphite in transmission fluid

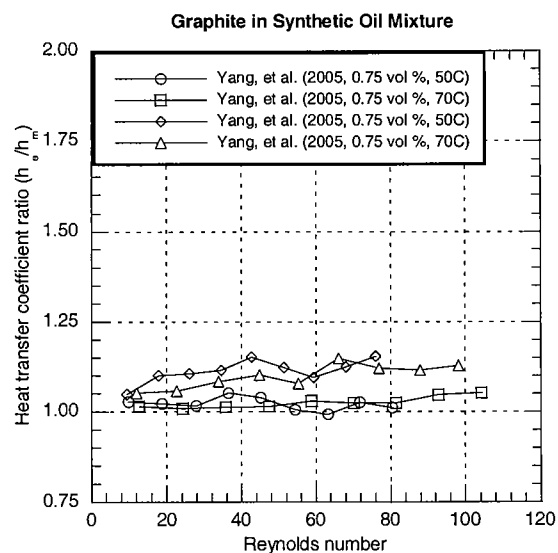


Figure 34. Laminar flow heat transfer of graphite in synthetic oil mixture

The results of Figures 33 and 34 show a weak temperature trend. The heat transfer enhancement is seen to decrease with increased temperature – a trend that is opposite that for thermal conductivity. However, the temperature range reported is small, and the temperature dependency shown is weak. Clearly, more test information is needed to define this trend.

6.2. Heat Transfer Enhancement in Turbulent Flow

Heat transfer results were available for turbulent flow of nanofluids from only two groups. The heat transfer enhancement results shown in Figures 35, 36, and 37 are for water-based nanofluids containing Al_2O_3 , TiO_2 , and Cu particles, respectively. The trends are similar in all three figures. There is little or no effect of Reynolds number on the heat transfer enhancement, and the enhancement increases with increased particle volume concentration. The heat transfer enhancement is the highest for Cu particles, followed by Al_2O_3 particles and then TiO_2 particles at the same volume concentration levels. From the standpoint of thermal conductivity, it is not surprising that the Cu-in-water nanofluid shows the highest heat transfer enhancement. However, the thermal conductivity enhancements for Al_2O_3 and TiO_2 in water are comparable and do not reflect the difference in the heat transfer enhancement shown in Figures 35 and 36. As noted above, the data are sparse, and more corroboration among experimenters is needed to establish the heat transfer enhancement trend with turbulent flow as a function of particle type.

For turbulent flow, some researchers have used a correlation calculation to compare heat transfer enhancement to thermal conductivity enhancement. By using a long-standing heat transfer correlation for turbulent flow, like the Dittus-Boelter correlation (1930), one can predict the Nusselt number of the base fluid with reasonable accuracy. Then, using the increased thermal conductivity of the nanofluid in the same Dittus-Boelter correlation as a rough simulation of the nanofluid, one can predict a Nusselt number for the nanofluid. In so doing, the Dittus-Boelter correlation (or its equivalent) often underpredicts the measured nanofluid Nusselt number. For heated turbulent flow, the base-fluid

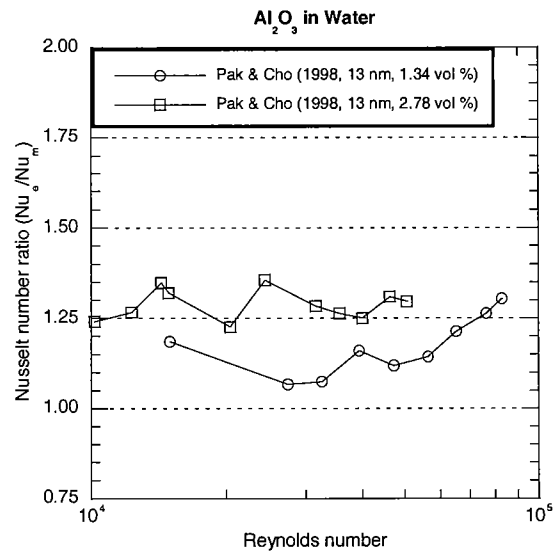


Figure 35. Turbulent flow heat transfer of Al_2O_3 in water

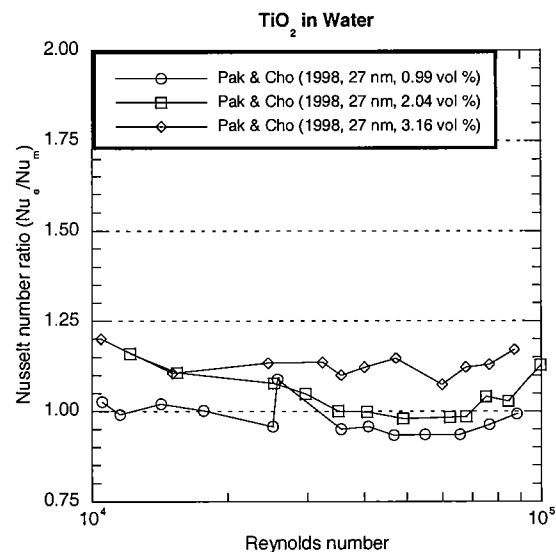


Figure 36. Turbulent flow heat transfer of TiO_2 in water

Nusselt number is proportional to the thermal conductivity to the 0.6 power. Thus, even if the enhancement ratios for thermal conductivity and Nusselt number were the same, the actual heat transfer would exceed the prediction for the heat transfer correlation because the thermal conductivity in it appears to only the 0.6 power. As noted previously, some authors have attributed the increased heat transfer enhancement above the thermal conductivity enhancement to particle-fluid interactions.

It is notable that the data for both turbulent and laminar flow are insufficient to determine a trend for heat transfer enhancement as a function of particle size. The thermal conductivity enhancement was seen to increase with particle size, but more experiments are required to establish such a trend with regard to heat transfer enhancement.

6.3. Heat Transfer Enhancement in Pool Boiling

Results are available from a few experiments for the pool boiling of nanofluids as listed in Table 3 of Appendix A. Heat transfer results are given in Figure 38 for Al_2O_3 in water boiling on the outside of small diameter tubes. The heat transfer enhancement ratio is below unity in all cases. The results are scattered with respect to particle size, but the enhancement ratio decreases as particle volume concentration increases, in contrast to the thermal conductivity enhancement results. The experimenters of Figure 38 noted particle coating on the heat surfaces, and they concluded that the poor nanofluid performance was due to particles coming out of suspension and depositing on the heated surfaces. Although the addition of particles to the base fluid is seen in Figure 38 to decrease the heat transfer rate, some experiments have shown an enhancement of critical heat flux above 1.0 (to be discussed subsequently). This effect of critical heat flux may compensate for the poor heat transfer enhancement results in some applications. (Generally, Nusselt numbers of boiling heat transfer are very high compared with those of single-phase heat transfer, and a reduction due to particle addition can have a minor effect on the overall heat transfer coefficient.)

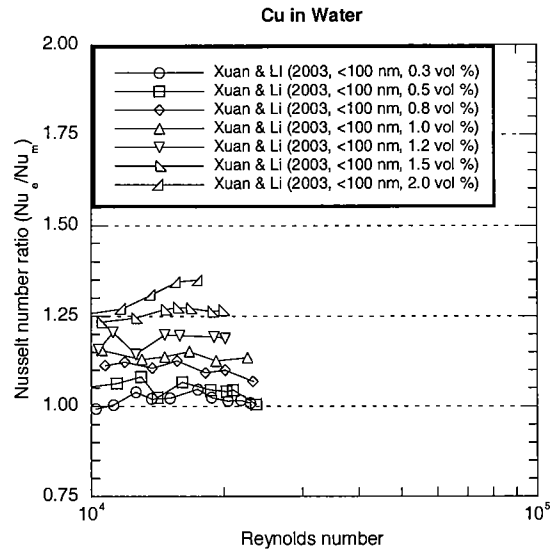


Figure 37. Turbulent flow heat transfer of Cu in water

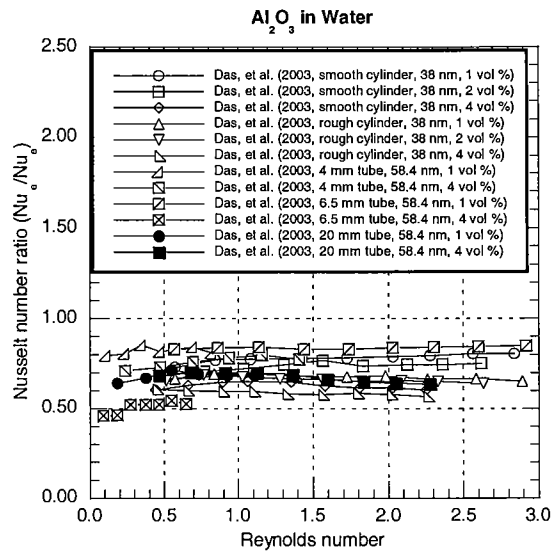


Figure 38. Pool-boiling heat transfer of Al_2O_3 in water

Additional heat transfer data for pool boiling of Al_2O_3 in water are given in Figure 39. Here the data from two groups are shown – both boiling from horizontal surfaces. The experimental parameters used by Bang and Chang (2005) in Figure 39 are in the same range as those of Figure 38, and the heat transfer results are similar. The addition of particles to the base fluid decreased the heat transfer rate, and the degradation became worse (lower ratio for the heat transfer coefficient enhancement in Figure 39) as particle volume concentration increased. This trend is opposite to that of the thermal conductivity enhancement. However, at very low particle volume concentrations (below 0.32%), the work of Wen and Ding (2005) shows heat transfer enhancement for pool boiling of this nanofluid. Also, the usual trend is observed in their data wherein heat transfer enhancement increases with increased particle volume concentration up to 0.32%. These results give a clear direction for future pool-boiling experimentation in the small volume concentration range, where positive heat transfer enhancement may be achieved.

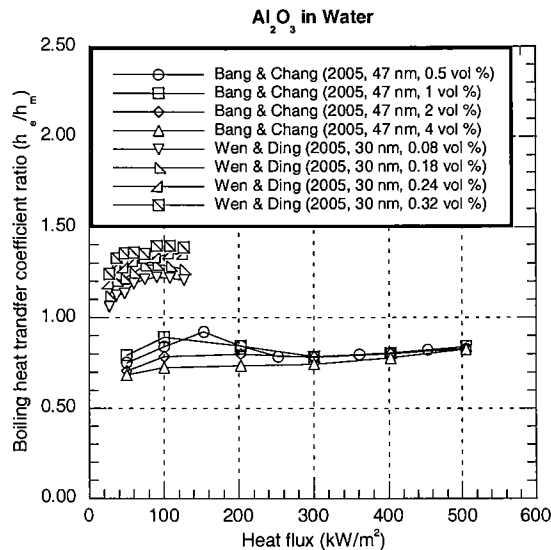


Figure 39. Pool-boiling heat transfer of Al_2O_3 in water from a horizontal surface

6.4. Critical Heat Flux Enhancement in Pool Boiling

The critical heat flux in pool boiling marks the beginning of the transition to vapor blanketing with low heat transfer coefficient and often high surface temperature. As such, the critical heat flux is often a limiting condition in industrial pool-boiling applications. It is often desirable to have this condition met far from the system operating range. Thus, any increase in the critical heat flux is usually a welcome condition, and nanofluids have been shown to provide such a condition. The results from the five experimental groups listed in Table 4 of Appendix A show an increase of nanofluid critical heat flux over the base fluid, i.e. values of the critical heat flux enhancement ratio above 1.0.

Figure 40 shows the critical heat flux enhancement of Al_2O_3 in water for pool boiling. The particle volume concentration range tested by the two groups is very large,

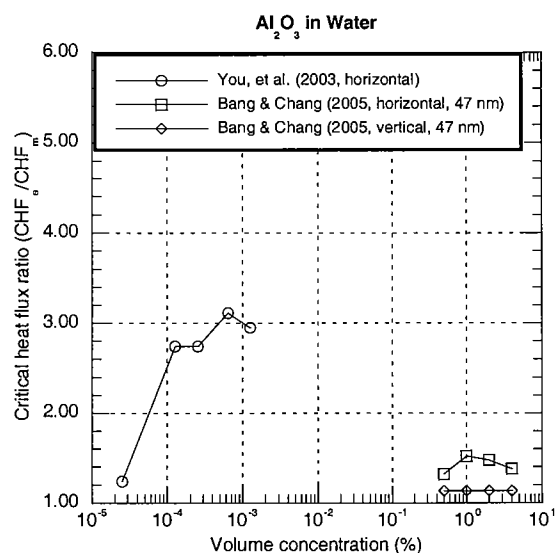


Figure 40. Critical heat flux of Al_2O_3 in water from a flat surface

and the enhancement ratio is above unity in all cases. However, high enhancement (up to 200%) was reached at very low particle volume concentrations (between 0.0001 and 0.001). This result is consistent with the heat transfer enhancement results for pool boiling, where very low particle volume concentrations produced the best results.

At relatively high particle volume concentrations, the critical heat flux enhancement is about the same for Al_2O_3 and CuO in water, as demonstrated by comparing Figures 40 and 41. However, this enhancement is modest with respect to the very high values obtained for Al_2O_3 in water (Figure 40) at very low particle volume concentrations ($<10^{-3}$ vol. %).

Figure 42 shows the critical heat flux enhancement for SiO_2 in water at relatively high particle volume concentrations, as reported by two experimental groups. The data of Vassallo et al. (2004) cover a large range of particle diameter (15 to 3000 nm). The critical heat flux enhancement results for the lowest and highest diameters are similar in magnitude and consistent with the high volume concentration results of Figures 40 and 41. (The result for 50 nm, which is closest to the particle sizes of Figures 40 and 41, is inconsistent with all the others.)

Also shown in Figure 42 is critical heat flux enhancement as a function of fluid acidity. Opposite to the case of thermal conductivity enhancement, a decrease in acidity increases the critical heat flux enhancement by as high as 350%.

The increased critical heat flux produced by nanofluids is very important for providing a safety margin for boiling heat transfer systems in the transportation industry, as well as other industries. The very high ratios reported for the critical heat flux enhancement are attractive for such systems and point to the direction for future research. However, flowing fluid heat transfer, both single phase and two phase, is most important to the transportation industry, and engine

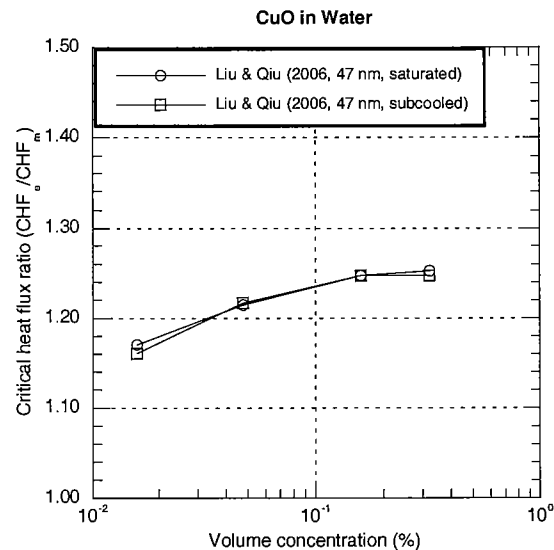


Figure 41. Critical heat flux of CuO in water from a jet on horizontal surface

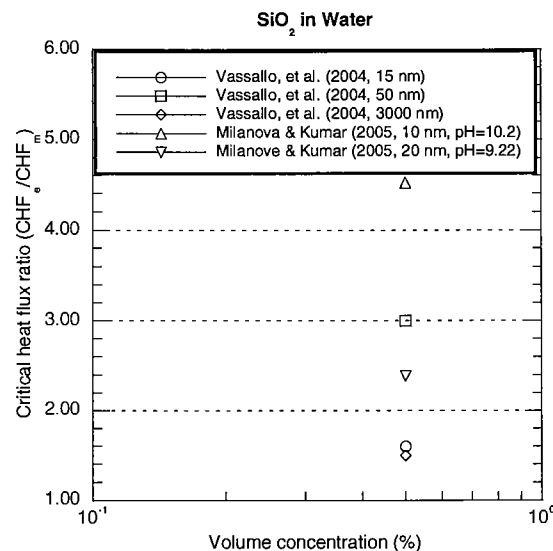


Figure 42. Critical heat flux of SiO_2 in water from a horizontal NiCr wire

cooling is a very important application in this area. Thus, it is important to extend the pool boiling work to flow boiling of nanofluids.

7. Experimental Research on Nanofluid Erosion

As mentioned previously, an important consideration in any particle-laden flow is the effect of erosion of material surfaces due to fluid motion. Although the nanoscale of the particles involved in nanofluids tends to mitigate particle erosion problems, it is a mechanism that needs detailed study. Nanoparticles tend to follow fluid streamlines better than larger particles suspended in flows; however, each application can have unique flow situations. Application-dependent parameters that can affect surface erosion include varying velocities, vortices, surface materials, particle characteristics, and operating requirements such as long or short term, steady-state or frequent transients, etc. For transportation industry applications, experiments are in progress, and preliminary results are available in a study by Routbort and Singh (2007). This study has application to vehicular radiators and measured erosion for CuO-in-ethylene glycol nanofluids impacting on 3003 aluminium. High velocities were used to simulate long-term tests. It is expected that the erosion rate will depend on the kinetic energy (size, density, and impact velocity) of the nanoparticles, as well as the angle of impact and the target material. Preliminary results with the CuO-in-ethylene glycol nanofluids were encouraging, showing very low erosion of the aluminium. However, significant material erosion of polymer pump gears, 0.7% weight loss after 1500 hours, illustrates the importance of material choices. Also, erosion from the impact of nanofluids with carbon nanotubes (aspect ratio of approximately 2000:1) was unacceptable for radiator use, leading to severe coating of all surfaces.

8. Theoretical Modeling of Nanofluids

For the purpose of theoretical modeling, a nanofluid can be defined as a mixture consisting of a continuous base fluid component called the “matrix” and a discontinuous solid component called “particles.” The properties, especially the thermal conductivity and viscosity, of nanofluids depend on their microstructures, such as the component properties, component volume concentrations, particle size, particle shape, particle distribution, particle motion, and matrix-particle interfacial effects. It is impossible to estimate the effective properties of nanofluids unless all the details of their microstructures are completely known. To avoid this problem, modelers usually estimate the effective properties based on some reasonable assumptions on the microstructures of the mixtures. In this section, the classical models for mixtures and new improvements in nanofluids are presented.

8.1. Density and Specific Heat

The calculation of the effective density ρ_e and the effective specific heat C_{pe} of a nanofluid is straightforward. They can be estimated based on the physical principle of the mixture rule as

$$\rho_e = \left(\frac{m}{V} \right)_e = \frac{m_m + m_p}{V_m + V_p} = \frac{\rho_m V_m + \rho_p V_p}{V_m + V_p} = (1 - v_p) \rho_m + v_p \rho_p \quad (1)$$

$$\begin{aligned} (\rho C_p)_e &= \rho_e \left(\frac{Q}{m \Delta T} \right)_e = \rho_e \frac{Q_m + Q_p}{(m_m + m_p) \Delta T} = \rho_e \frac{(m C_p)_m \Delta T + (m C_p)_p \Delta T}{(m_m + m_p) \Delta T} \\ &= \rho_e \frac{(\rho C_p)_m V_m + (\rho C_p)_p V_p}{\rho_m V_m + \rho_p V_p} = (1 - v_p) (\rho C_p)_m + v_p (\rho C_p)_p \end{aligned} \quad (2)$$

which can be rewritten as

$$C_{pe} = \frac{(1 - v_p) (\rho C_p)_m + v_p (\rho C_p)_p}{(1 - v_p) \rho_m + v_p \rho_p} \quad (3)$$

8.2. Thermal Conductivity

Maxwell was one of the first to analytically investigate conduction through suspended particles. Maxwell (1873) considered a very dilute suspension of spherical particles by ignoring the interactions among the particles. The Maxwell equation can be obtained by solving the Laplace equation for the temperature field outside the particles in two ways: considering a large sphere containing all the spherical particles with an effective thermal conductivity k_e embedded in a matrix with a thermal conductivity k_m or considering all the spherical particles with a thermal conductivity k_p embedded in a matrix with a thermal conductivity k_m . The resulting equation is

$$k_e = k_m + 3v_p \frac{k_p - k_m}{2k_m + k_p - v_p(k_p - k_m)} k_m \quad (4)$$

Note that the Maxwell equation is only a first-order approximation and applies only to mixtures with low particle volume concentrations.

A great number of extensions to the Maxwell equation have been carried out ever since Maxwell's initial investigation. These extensions take into account various factors related to effective thermal conductivity, including

- particle shape (Fricke 1924; Fricke 1953; Polder and van Santen 1946; Taylor 1965; Taylor 1966; Hamilton and Crosser 1962; Granqvist and Hunderi 1977; Granqvist and Hunderi 1978; Xue 2000),
- particle distribution (Rayleigh 1892; Wiener 1912),
- high volume concentration (Bruggeman 1935; Böttcher 1945; Landauer 1952; Jeffrey 1973; Davis 1986),
- particle-shell structure (Kerner 1956; van de Hulst 1957; Pauly and Schwan 1959; Schwan, et al. 1962; Lamb, et al. 1978; Benveniste and Miloh 1991; Lu and Song 1996; Xue 2000), and
- contact resistance (Benveniste 1987; Hasselman and Johnson 1987).

Some of these equations are summarized in Table 5 of Appendix B.

While these equations predict thermal conductivity reasonably well for dilute mixtures of relatively large particles in fluids, the comparison between experimental data and theoretical predictions for nanofluids is generally not satisfactory. These equations either underpredict experimental data for nanofluids containing spherical particles or overpredict experimental data for nanofluids containing prolate spheroids with $a \gg b = c$ (such as nanotubes). To improve the predictions, mechanisms have been identified and formulated specifically for the nanoscale, including the effects of nanoparticle-matrix interfacial layer, nanoparticle Brownian motion, and nanoparticle cluster/aggregate.

8.2.1. Effect of Nanoparticle-Matrix Interfacial Layer

Liquid molecules close to a solid surface are known to form layered structures (Henderson and Swol 1984; Yu, et al. 2000). With these solid-like liquid layers, the nanofluid structure consists of solid nanoparticles, shells (solid-like liquid layers), and a bulk liquid. Because the layered molecules are in an intermediate physical state between a solid and a bulk liquid (Yu, et al. 2000), the solid-like layer of liquid molecules would be expected to lead to a higher thermal conductivity than that of the bulk liquid. Therefore, the solid-like liquid layer acts as a thermal bridge between a solid particle and a bulk liquid. Based on this assumption, Yu and Choi (2003) have modified the Maxwell equation for the effective thermal conductivity of spherical particle-liquid suspensions to include the effect of this ordered liquid layer

$$k_e = k_m + 3v_c \frac{k_c - k_m}{2k_m + k_c - v_c(k_c - k_m)} k_m \quad (5)$$

where the thermal conductivity k_c of the particle-shell structured complex particles can be estimated from the Maxwell equation (Miles and Roberson 1932)

$$k_c = k_s + 3v_r \frac{k_p - k_s}{2k_s + k_p - v_r(k_p - k_s)} k_s \quad (6)$$

This idea can be extended to nonspherical particles. By modifying the Hamilton and Crosser equation (1962), Yu and Choi (2004) obtained an effective thermal conductivity equation for ellipsoid-shell-liquid nanofluids

$$k_e = k_m + \Psi^{-1} v_c \sum_{a,b,c} \frac{k_{ci} - k_m}{(3\Psi^{-1} - 1)k_m + k_{ci} - v_c(k_{ci} - k_m)} k_m \quad (7)$$

where the sphericity Ψ of the particle is defined as the ratio of the surface area of a sphere, with a volume equal to that of the particle, to the surface area of the particle. The thermal conductivity k_{ci} ($i = a, b, c$) of the ellipsoid-shell structured complex particles can be estimated by the following equation (Bilboul 1969)

$$k_{ci} = k_s + v_r \frac{k_p - k_s}{k_s + (d_{pi} - v_r d_{ci})(k_p - k_s)} k_s \quad (8)$$

where the depolarization factors d_i ($i = a, b, c$) are defined by

$$d_i = \frac{abc}{2} \int_0^\infty \frac{1}{(i^2 + w)\sqrt{(a^2 + w)(b^2 + w)(c^2 + w)}} dw \quad (9)$$

The shell thermal conductivity k_s is dependent on the nature of the particle-liquid interfacial effect. Assuming that the thermal conductivity of the solid-like liquid layer changes linearly from the liquid thermal conductivity at its outside surface to the particle thermal conductivity at its inside surface, Xie et al. (2005) and Ren et al. (2005) obtained the thermal conductivity k_s of the solid-like liquid layer from the averaging equivalent principle

$$k_s = \frac{(k_p - v_r^{1/3} k_m)^2}{(1 - v_r^{1/3})(k_p - v_r^{1/3} k_m) + v_r^{1/3}(k_p - k_m) \ln\left(\frac{k_p}{v_r^{1/3} k_m}\right)} \quad (10)$$

The shell volume fraction v_s also has to be estimated from the characteristics of the particle-liquid interfacial layer.

8.2.2. Effect of Nanoparticle Brownian Motion

The Brownian motion of nanoparticles, because of their size, is another potential factor in calculating the thermal conductivity enhancement of nanofluids. In most cases, the effect of Brownian motion of suspended nanoparticles in nanofluids can be considered as an addition to the enhanced thermal conductivity predicted by classical equations. Based on this concept, Xuan et al. (2003) proposed the following modification to the Maxwell equation

$$k_e = k_m + 3v_p \frac{k_p - k_m}{2k_m + k_p - v_p(k_p - k_m)} k_m + \frac{1}{2} \rho_p C_{pp} v_p \sqrt{\frac{k_B T}{3\pi\mu_m r_c}} \quad (11)$$

It should be noted that this equation includes the cluster effect through the cluster gyration radius r_c , which needs to be determined empirically.

Jang and Choi (2004) also developed a dynamic model that takes into account convection induced by a single Brownian nanoparticle. Their model can be expressed as a modification to the parallel mixture rule

$$k_e = (1 - v_p)k_m + v_p k_p + 3c(r_m/r_p)v_p \left(\frac{k_B T}{3\pi\mu_m v_m l_m} \right)^2 \text{Pr} k_m \quad (12)$$

The parallel distribution of nanoparticles is very unlikely for practical nanofluids, and the empirical parameter c in the equation is another limiting factor for it to be used in predicting the effective thermal conductivity of nanofluids.

Efforts were also made to predict the effective thermal conductivity with the nanoparticle Brownian motion effect for particular nanofluids. Using this approach, Koo and Kleinstreuer (2004) developed an effective thermal conductivity model for CuO-based nanofluids

$$k_e = k_m + 3v_p \frac{k_p - k_m}{2k_m + k_p - v_p(k_p - k_m)} k_m + 5 \times 10^4 \beta \rho_m C_{pm} v_p \sqrt{\frac{k_B T}{2\rho_p r_p}} [(-134.63 + 1722.3v_p) + (0.4705 - 6.04v_p)T] \quad (13)$$

which is a modification to the Maxwell equation. The parameter β is related to nanoparticle Brownian motion and was determined empirically as

$$\beta = \begin{cases} 0.0137(100v_p)^{-0.8229} & v_p < 0.01 \\ 0.0011(100v_p)^{-0.7272} & v_p > 0.01 \end{cases} \quad (14)$$

The nanoparticle Brownian motion effect can also be considered as a correction factor to the enhanced thermal conductivity predicted by classical equations. The following equation is an example of this approach

$$k_e = \left[1 + cv_p \left(\frac{9k_B T}{\pi \rho_p v_m^2 r_p} \right)^m \text{Pr}^{0.333} \right] \left\{ k_m + 3v_p \frac{k_p^R}{2k_m + k_p^R - v_p (k_p^R - k_m)} k_m \right\} \quad (15)$$

where c and m are empirical parameters. This equation is a modification to the Maxwell equation, adding a contact resistance effect, and was proposed by Prasher et al. (2005, 2006a).

8.2.3. Effect of Nanoparticle Cluster/Aggregate

Nanoparticles commonly form cluster/aggregate structures in nanofluids. These cluster/aggregate structures act like local percolation structures and, therefore, add to the effective thermal conductivity enhancement of nanofluids. Wang et al. (2003) took this cluster effect into account by introducing a cluster radius distribution function $n(r)$. The resulting equation is a modification to the Maxwell equation

$$k_e = k_m + \frac{3v_p \int_0^\infty \frac{k_p(r) - k_m}{2k_m + k_p(r)} n(r) dr}{(1 - v_p) + 3v_p \int_0^\infty \frac{k_m}{2k_m + k_p(r)} n(r) dr} k_m \quad (16)$$

where the cluster radius distribution function is estimated approximately by a log-normal distribution of the form

$$n(r) = \frac{1}{\sqrt{2\pi} (\ln \sigma) r} e^{-[\ln(r/r_p)/(\sqrt{2\pi} \ln \sigma)]^2} \quad (17)$$

and the standard deviation σ can take the classical value of 1.5 (Wang, et al. 2003).

Prasher et al. (2006b) also pointed out that the thermal conductivity of nanofluids based purely on conduction phenomenon can be significantly enhanced as a result of aggregation of the nanoparticles. They proposed the following equation to include the nanoparticle aggregate effect

$$k_e = k_m + 3(r_a/r_p)^{3-d_f} v_p \frac{k_a - k_m}{2k_m + k_a - (r_a/r_p)^{3-d_f} v_p (k_a - k_m)} k_m \quad (18)$$

which can also be considered as a modification to the Maxwell equation. Prasher et al. (2006b) suggested using the Bruggeman equation (1935) to estimate the aggregate thermal conductivity k_a

$$\left[1 - (r_p/r_a)^{3-d_f}\right] \frac{k_m - k_a}{2k_a + k_m} + (r_p/r_a)^{3-d_f} \frac{k_p - k_a}{2k_a + k_p} = 0 \quad (19)$$

Nanoparticle cluster/aggregate structures in nanofluids are positive factors to the effective thermal conductivity enhancement. Nonetheless, the large nanoparticle cluster/aggregate structures that form tend to settle out of the nanofluids, thereby eliminating the effective thermal conductivity enhancement. From this point of view, the nanoparticle cluster/aggregate size is critical to the thermal performance of nanofluids.

8.2.4. Nanofluids Containing Carbon Nanotube Particles

Generally, carbon nanotube particles can be considered as prolate spheroids that satisfy $a \gg b = c$. Therefore, many models developed for prolate spheroid suspensions can be used for estimating the effective thermal conductivity of carbon nanotube-based nanofluids. Using this approach, Nan et al. (2004) proposed the following approximate equation obtained from the Fricke equation (1924; 1953) under the condition that k_p^R is much larger than k_m

$$k_e = k_m + \frac{1}{3} v_p \frac{k_p}{1 + Rk_p/a} \quad (20)$$

which includes the contact resistance effect and can be reduced, for zero contact resistance, to (Nan, et al. 2003)

$$k_e = k_m + \frac{1}{3} v_p k_p \quad (21)$$

Even though this model predicts the experimental data of the carbon nanotube suspensions reasonably well, a physical basis is lacking for the assumption of a series distribution along the longitudinal direction, which was used to obtain the equivalent particle thermal conductivity k_p^R .

The depolarization factor equals 0 and 1/2 when the carbon nanotube particles are parallel and perpendicular to the applied field, respectively. Based on this fact, Xue (2005) introduced a distribution function $P(w)$ instead of the equal probability average and derived the following equation for carbon nanotube-based nanofluids

$$k_e = k_m + \frac{\frac{4}{\pi} v_p \frac{k_p - k_m}{\sqrt{k_m k_p}} \arctan \sqrt{\frac{k_p}{k_m}}}{(1 - v_p) + \frac{4}{\pi} v_p \frac{k_m}{\sqrt{k_m k_p}} \arctan \sqrt{\frac{k_p}{k_m}}} k_m \quad (22)$$

for a normal-like distribution $P(w) = (2/\pi)\sqrt{w(1-w)}$, and

$$k_e = k_m + \frac{2v_p \ln\left(\frac{k_p + k_m}{2k_m}\right)}{(1 - v_p) + 2v_p \frac{k_m}{k_p - k_m} \ln\left(\frac{k_p + k_m}{2k_m}\right)} k_m \quad (23)$$

for a uniform distribution $P(w) = 2$.

The above discussions imply that the mathematical models based on the physical mechanisms of the nanoparticle-matrix interfacial layer effect, nanoparticle Brownian motion effect, or nanoparticle cluster/aggregate effect usually involve some empirical parameters. These empirical parameters have to be determined first before the mathematical models can be used to predict the effective thermal conductivity of a nanofluid. This requirement greatly limits model usage. Also, instead of one pure mechanism, the combined effect of these and other mechanisms often contributes to the effective thermal conductivity enhancement of a nanofluid. This issue remains to be addressed in future research on the physical mechanisms and mathematical models of the effective thermal conductivity enhancements of nanofluids.

8.3. Viscosity

The history of the study on the effective viscosity of particle-liquid mixtures is almost as long as the one on the effective thermal conductivity. Einstein was the first to calculate the effective viscosity of a suspension of spheres on the basis of the phenomenological hydrodynamic equations. In his elegant paper, Einstein (1906) evaluated the effective viscosity μ_e of a linearly viscous fluid of viscosity μ_m containing a dilute suspension of small particles. By assuming that the disturbance of the flow pattern of the matrix base fluid caused by a given particle does not overlap with the disturbance of flow caused by the presence of a second suspended particle, Einstein derived the following equation

$$\mu_e = (1 + 2.5v_p)\mu_m \quad (24)$$

Ever since Einstein's initial work, researchers have made progress in extending the Einstein theory in three major areas. The first is to extend the Einstein equation to higher particle volume concentrations by taking some of the particle-particle interactions into account. This type of theoretical equation for the effective viscosity of a mixture can usually be expressed as (Liu and Masliyah 1996)

$$\mu_e = (1 + c_1v_p + c_2v_p^2 + c_3v_p^3 + \dots)\mu_m \quad (25)$$

The second extension takes into account the fact that the effective viscosity of a mixture becomes infinite at the maximum particle packing volume concentration $v_{p\max}$. This theoretical equation usually has the term $[1 - (v_p/v_{p\max})]^\alpha$ in the denominator, and it can be expressed in a form similar to Equation 25. From a practical application viewpoint, the predictions from these

two extensions are basically the same as from the original Einstein equation because of the very low particle volume concentrations.

The third extension is for non-spherical particle suspensions. Some of these equations are included in Table 6 of Appendix B.

Experimental data for the effective viscosity of nanofluids are limited to certain nanofluids, such as

- Al_2O_3 in water (Pak and Cho 1998; Das, et al. 2003b; Putra, et al. 2003; Li, et al. 2005; Heris, et al. 2006),
- CuO in water (Heris, et al. 2006; Kulkarni, et al. 2006),
- TiO_2 in water (Pak and Cho 1998),
- MWCNT in water (Ding, et al. 2006), and
- Al_2O_3 in octane (Liu, et al. 2006).

The ranges of the parameters (the particle volume concentration, temperature, etc.) are also limited. Still, the experimental data show the trend that the effective viscosities of nanofluids are higher than the theoretical predictions. In an attempt to rectify this situation, researchers proposed equations applied to specific applications, e.g., Al_2O_3 in water (Maïga, et al. 2004), Al_2O_3 in ethylene glycol (Maïga, et al. 2004), and TiO_2 in water (Tseng and Lin 2003). Kulkarni et al. (2006) proposed an equation for CuO in water that takes temperature into account. The problem with these equations is that they do not reduce to the Einstein equation at very low particle volume concentrations and, therefore, lack a sound physical basis.

8.4. Heat Transfer Coefficient

Since the heat transfer performance is a better indicator than the effective thermal conductivity for nanofluids used as coolants in transportation and other industries, the modeling of nanofluid heat transfer coefficients is gaining attention from researchers. However, as can be seen from Table 7 of Appendix B, it is still at an early stage, and the theoretical models for nanofluid heat transfer coefficients are quite limited. All the equations are modified from traditional equations such as the Dittus-Boelter equation (1930) or the Gnielinski equation (1976) with empirical parameters added. Therefore, these equations are only valid for certain nanofluids in small parameter ranges. More experimental and theoretical studies are needed before general models can be developed and verified.

8.5. Simulation

Limited computer simulations of the thermal properties and heat transfer characteristics of nanofluids have been performed. While some of these simulations dealt with the effective thermal properties of nanofluids, such as the effective thermal conductivity (Bhattacharya, et al. 2004; Xue, et al. 2004) or the effective viscosity (Pozhar 2000), most of them focused on the heat transfer of nanofluids (Gupte, et al. 1995; Sato, et al. 1998; Ali, et al. 2003; Khanafer, et al. 2003; Ali, et al. 2004; Gosselin and da Silva 2004; Kim, et al. 2004; Maïga, et al. 2004; Roy, et al. 2004; Shenogin 2004; Ding and Wen 2005; Khaled and Vafai 2005; Koo and Kleinstreuer

2005; Kumar and Murthy 2005; Maïga, et al. 2005; Wen and Ding 2005a; Xuan and Yao 2005; Evans, et al. 2006; Jou and Tzeng 2006; Koblinski and Thomin 2006; Kim, et al. 2006; Mansour, et al. 2006; Prasher, et al. 2006c). While the computer simulations give some general implications of thermal properties and heat transfer of nanofluids, detailed quantitative results require more verified experimental data and theoretical models.

9. Applications of Nanofluids

Nanofluids can be used to improve heat transfer and energy efficiency in a variety of thermal systems, including the important application of vehicle cooling. Much of the work in the field of nanofluids is being done in national laboratories and academia and is at a stage beyond discovery research. Recently, the number of companies that see the potential of nanofluid technology and are in active development work for specific industrial applications is increasing. In the transportation industry, GM and Ford, among others, have ongoing nanofluid research projects. In this section some examples of actual and potential applications will be discussed for transportation, as well as microelectronics, defense, nuclear, space, and biomedical.

9.1. Transportation

Ethylene glycol and water mixture, the nearly universally used automotive coolant, is a relatively poor heat transfer fluid compared to water alone. Engine oils perform even worse as a heat transfer medium. The addition of nanoparticles to the standard engine coolant has the potential to improve automotive and heavy-duty engine cooling rates. Such improvement can be used to remove engine heat with a reduced-size coolant system. Smaller coolant systems result in smaller and lighter radiators, which in turn benefit almost every aspect of car and truck performance and lead to increased fuel economy. Alternatively, improved cooling rates for automotive and truck engines can be used to remove more heat from higher horsepower engines with the same size of coolant system.

A promising nanofluid engine coolant is pure ethylene glycol with nanoparticles. Pure ethylene glycol is a poor heat transfer fluid compared to a 50/50 mixture of ethylene glycol and water, but the addition of nanoparticles will improve the situation. If the resulting heat transfer rate can approach the 50/50 mixture rate, there are important advantages. Perhaps one of the most prominent is the low-pressure operation of an ethylene-glycol-based nanofluid compared with a 50/50 mixture of ethylene glycol and water. An atmospheric-pressure coolant system has lower potential capital cost. This nanofluid also has a high boiling point, which is desirable for maintaining single-phase coolant flow. In addition, a higher boiling point coolant can be used to increase the normal coolant operating temperature and then reject more heat through the existing coolant system. More heat rejection allows a variety of design enhancements, including engines with higher horsepower.

The results of nanofluid research are being applied to the cooling of automatic transmissions. Tzeng et al. (2005) dispersed CuO and Al₂O₃ nanoparticles into engine transmission oil. The experimental platform was the transmission of a four-wheel-drive vehicle. The transmission had an advanced rotary blade coupling, where high local temperatures occurred at high rotating speeds. For that reason, improved heat transfer rates from the transmission fluid were important. The temperature distribution on the exterior of the rotary-blade-coupling transmission was measured at four engine operating speeds (400, 800, 1200, and 1600 rpm), and the optimum composition of nanofluids with regard to heat transfer performance was investigated. The results showed that CuO nanofluids produced the lowest transmission temperatures both at high and low rotating speeds. Thus, use of nanofluid in the transmission has a clear advantage from the

thermal performance viewpoint. As in all nanofluid applications, however, consideration must be given to such factors as particle settling, particle agglomeration, and surface erosion.

In automotive lubrication applications, surface-modified nanoparticles stably dispersed in mineral oils are reported to be effective in reducing wear and enhancing load-carrying capacity (Zhang and Que 1997). Recent results from a research project involving industry and a university points to the use of nanoparticles in lubricants to enhance tribological properties such as load-carrying capacity, wear resistance, and friction reduction between moving mechanical components. Such results are encouraging for improving heat transfer rates in automotive systems through the use of nanofluids.

9.2. Electronics Cooling

The power density of integrated circuits and microprocessors has increased dramatically in recent years. The trend should continue for the foreseeable future. Recently, the International Technology Roadmap for Semiconductors projected that, by 2018, high-performance integrated circuits will contain more than 9.8 billion transistors on a chip area of 280 mm^2 – more than 40 times as many as on today's chips of 90-nm node size. Future processors for high-performance computers and servers have been projected to dissipate higher power in the range of 100-300 W/cm^2 . Whether these values actually become reality is not as significant as the projection that the general trend to higher power density electronics will continue. Existing air-cooling techniques for removing this heat are already reaching their limits, and liquid cooling technologies are being, and have been, developed for replacing them. Single-phase fluids, two-phase fluids, and nanofluids are candidate replacements for air. All have increased heat transfer capabilities over air systems, and all are being investigated.

Nanofluids have been considered as the working fluid for heat pipes in electronic cooling applications. Tsai et al. (2004) used a water-based nanofluid as the working medium in a circular heat pipe designed as a heat spreader to be used in a CPU in a notebook or a desktop PC. The results showed a significant reduction in thermal resistance of the heat pipe with the nanofluid as compared with deionized water. The measured results also showed that the thermal resistance of a vertical meshed heat pipe varies with the size of nanoparticles. In a related study, Ma et al. (2006) investigated the effect of nanofluids on the heat transport capability of an oscillating heat pipe. Experimental results showed that, at the input power of 80 W, a nanofluid containing 1 vol. % nanoparticles reduced the temperature difference between the evaporator and the condenser from 40.9°C to 24.3°C . These positive results are promoting the continued research and development of nanofluids for such applications.

9.3. Defense

A number of military devices and systems require high-heat-flux cooling to the level of tens of MW/m^2 . At this level, cooling with conventional fluids is challenging. Examples of military applications include cooling of power electronics and directed-energy weapons. Directed-energy weapons involve high heat fluxes ($>500\text{-}1000 \text{ W}/\text{cm}^2$), and providing adequate cooling of them and the associated power electronics is a critical need. Nanofluids have the potential to provide the required cooling in such applications as well as in other military systems, including military

vehicles, submarines, and high-power laser diodes. In some cases, nanofluid research for defense applications includes multifunctional nanofluids with added thermal energy storage or energy harvesting through chemical reactions.

Transformer cooling is important to the Navy as well as the power generation industry with the objective of reducing transformer size and weight. The ever-growing demand for greater electricity production can lead to the necessity of replacing and/or upgrading transformers on a large scale and at a high cost. A potential alternative in many cases is the replacement of the conventional transformer oil with a nanofluid. Such retrofits can represent considerable cost savings. It has been demonstrated that the heat transfer properties of transformer oils can be significantly improved by using nanoparticle additives.

9.4. Space

You et al. (2003) and Vassalo et al. (2004) have reported order of magnitude increases in the critical heat flux in pool boiling with nanofluids compared to the base fluid alone. (This body of research was discussed in some detail previously.) Such levels present the possibility of raising chip power in electronic components or simplifying cooling requirements for space applications. High critical heat fluxes allow boiling to higher qualities with increased heat removal and wider safety margin from film boiling. This feature makes nanofluids attractive in general electronic cooling as well as space applications where power density is very high.

9.5. Nuclear Systems Cooling

The Massachusetts Institute of Technology has established an interdisciplinary center for nanofluid technology for the nuclear energy industry. Currently, they are evaluating the potential impact of the use of nanofluids on the safety, neutronic, and economic performance of nuclear systems.

9.6. Biomedicine

Nanofluids and nanoparticles have many applications in the biomedical industry. For example, to circumvent some side effects of traditional cancer treatment methods, iron-based nanoparticles could be used as delivery vehicles for drugs or radiation without damaging nearby healthy tissue. Such particles could be guided in the bloodstream to a tumor using magnets external to the body. Nanofluids could also be used for safer surgery by producing effective cooling around the surgical region and thereby enhancing the patient's chance of survival and reducing the risk of organ damage. In a contrasting application to cooling, nanofluids could be used to produce a higher temperature around tumors to kill cancerous cells without affecting nearby healthy cells (Jordan, et al. 1999).

9.7. Other Applications

There are unending situations where an increase in heat transfer effectiveness can be beneficial to the quality, quantity, and/or cost of a product or process. In many of these situations, nanofluids are good candidates for accomplishing the enhancement in heat transfer

performance. For example, nanofluids have potential application in buildings where increases in energy efficiency could be realized without increased pumping power. Such an application would save energy in a heating, ventilating, and air conditioning system while providing environmental benefits. In the renewable energy industry, nanofluids could be employed to enhance heat transfer from solar collectors to storage tanks and to increase the energy density. Nanofluid coolants also have potential application in major process industries, such as materials, chemical, food and drink, oil and gas, paper and printing, and textiles.

10. Concluding Remarks and Future Work

The vehicular transportation industry as well as many other industries has specific needs to increase heat transfer rates under a variety of constraints. Nanofluids have the potential to satisfy many such needs and constraints. For automotive-engine coolant applications, the important features of nanofluids are the high heat transfer coefficients for liquids with high boiling points and low pressures. These characteristics of nanofluids make them attractive for this and other automotive applications, as well as for a large number of other industries. Increased heat transfer rates in engines could reduce the required cooling system size or decrease the pumping power needs. However, ideal or even optimized nanofluids for automotive applications do not exist yet. This literature review has shown that the research into nanofluid thermal conductivity is far enough along to be able to identify reproducible trends from multiple researchers in many areas. Some parametric trends, such as particle size, still require substantiation, and the use of additives has barely been addressed. However, the thermal conductivity trends reviewed in this study generally agree with the heat transfer trends and provide application guidance, although the heat transfer data themselves are somewhat sparse. The existing results point to heat transfer enhancement in the range of 15-40% with readily available oxide nanoparticles in a variety of base fluids. The results also point to future research directions to achieve heat transfer enhancement of an order of magnitude. Both laminar and turbulent flow studies need to be expanded substantially and general correlation equations developed for use in industrial applications. Flow-boiling experiments should be added to the existing database.

As part of this study, general trends were identified in thermal conductivity and heat transfer established by the majority of researchers. However, several areas were identified where discrepancies exist. Comparing data among research groups involves inaccuracies due to the poor characterization of the nanofluids studied. It is difficult to measure the nanoparticle size, shape, and distribution in fluids. Often, the particle size was determined by a laser scattering technique that emphasizes the largest particles, and size distribution was not considered. A more advanced technique for these measurements is X-ray small angle scattering, which can potentially yield accurate measurements of particle size, distribution, and shape. In addition, viscosity measurement of the nanofluids could be a helpful parameter in comparing nanofluid results among research groups.

In any application of nanofluids, it is important to consider surface erosion caused by the flowing fluid as well as effects of particle settling and agglomeration. Erosion results are only starting to appear in the literature. The effects of agglomeration and settling need serious attention. The agglomeration of particles in a nanofluid is exacerbated by the two-step process of producing nanofluids where powders are added to liquids. The dispersion and suspension of nanoparticles in a fluid pose a difficult colloidal chemistry problem, and considerable work remains to be done if the two-step process is ever to develop into large-scale production. (The two-step process is currently the most economical way to produce nanofluids and has good potential for scale-up to commercial production levels.)

While many models have been proposed and simulations have been developed for nanofluid thermal properties, it is still not possible to specify a nanofluid for a particular application based on a general verified theory. Current theories generally fail to predict thermal conductivity

enhancement and its temperature dependence from the properties of materials. The current semi-empirical approach of experiments and correlation of results would benefit from guidance from fundamental theory.

In summary, the next steps in the nanofluid research cycle are to concentrate on heat transfer enhancement and its physical mechanisms, taking into consideration such items as the optimum particle size and shape, particle volume concentration, fluid additive, particle coating, and base fluid. Continued effort on thermal properties is important as well. Better characterization of nanofluids is also important for developing engineering designs based on the work of multiple research groups, and fundamental theory to guide this effort should be improved. Important features for commercialization must be addressed, including particle settling, particle agglomeration, surface erosion, and large-scale nanofluid production at acceptable cost.

Appendix A.

Compilation of Experimental Data on Nanofluids

Table 1. Thermal Conductivity Enhancements

| Author (Year) | Nanofluid | Concentration (vol %) | Particle Size (nm) | Enhancement (ratio) | Note |
|-----------------------------------|---|-----------------------|--------------------|---------------------|--|
| Masuda, et al. (1993) | Al ₂ O ₃ -water (31.85°C) | 1.30- 4.30 | 13 | 1.109-1.324 | two-step method temperature effect |
| | Al ₂ O ₃ -water (46.85°C) | 1.30- 4.30 | 13 | 1.100-1.296 | |
| | Al ₂ O ₃ -water (66.85°C) | 1.30- 4.30 | 13 | 1.092-1.262 | |
| | SiO ₂ -water (31.85°C) | 1.10- 2.30 | 12 | 1.010-1.011 | |
| | SiO ₂ -water (46.85°C) | 1.10- 2.30 | 12 | 1.009-1.010 | |
| | SiO ₂ -water (66.85°C) | 1.10- 2.40 | 12 | 1.005-1.007 | |
| | TiO ₂ -water (31.85°C) | 3.25- 4.30 | 27 | 1.080-1.105 | |
| | TiO ₂ -water (46.85°C) | 3.25- 4.30 | 27 | 1.084-1.108 | |
| | TiO ₂ -water (86.85°C) | 3.10- 4.30 | 27 | 1.075-1.099 | |
| Lee, et al. (1999) | Al ₂ O ₃ -water | 1.00- 4.30 | 38.4 | 1.073 -1.10 | two-step method |
| | CuO-water | 1.00- 3.41 | 23.6 | 1.03 -1.12 | |
| | Al ₂ O ₃ -ethylene glycol | 1.00- 5.00 | 38.4 | 1.03 -1.18 | |
| | CuO-ethylene glycol | 1.00- 4.00 | 23.6 | 1.05 -1.23 | |
| Wang, et al. (1999) | Al ₂ O ₃ -water | 3.00- 5.50 | 28 | 1.11 -1.16 | two-step method |
| | CuO-water | 4.50- 9.70 | 23 | 1.17 -1.34 | |
| | Al ₂ O ₃ -ethylene glycol | 5.00- 8.00 | 28 | 1.25 -1.41 | |
| | CuO-ethylene glycol | 6.20-14.80 | 23 | 1.24 -1.54 | |
| | Al ₂ O ₃ -engine oil | 2.25- 7.40 | 28 | 1.05 -1.30 | |
| | Al ₂ O ₃ -pump oil | 5.00- 7.10 | 28 | 1.13 -1.20 | |
| | Cu (+ laurate salt)-water | 2.50- 7.50 | 100 | 1.22 -1.75 | |
| Cu (+ oleic acid)-transformer oil | 2.50- 7.50 | 100 | 1.12 -1.43 | | |
| Choi, et al. (2001) | MWCNT (+ dispersant)-polyalphaolefin | 0.04- 1.02 | 25x50000 | 1.02 -2.57 | two-step method one-step physical method |
| | Cu (old)-ethylene glycol | 0.10- 0.56 | <10 | 1.016-1.100 | |
| | Cu (fresh)-ethylene glycol | 0.11- 0.56 | <10 | 1.031-1.140 | |
| Eastman, et al. (2001) | Cu (+ thioglycolic acid)-ethylene glycol | 0.01- 0.28 | <10 | 1.002-1.410 | two-step method |
| | SiC-water | 0.78- 4.18 | 26 sphere | 1.03 -1.17 | |
| | SiC-water | 1.00- 4.00 | 600 cylinder | 1.06 -1.24 | |
| | SiC-ethylene glycol | 0.89- 3.50 | 26 sphere | 1.04 -1.13 | |
| | SiC-ethylene glycol | 1.00- 4.00 | 600 cylinder | 1.06 -1.23 | |
| Xie, et al. (2002a) | Al ₂ O ₃ -water | 1.80- 5.00 | 60.4 | 1.07 -1.21 | two-step method solid crystalline phase effect morphology effect pH value effect base fluid effect |
| | Al ₂ O ₃ -ethylene glycol | 1.80- 5.00 | 15 | 1.06 -1.17 | |
| | Al ₂ O ₃ -ethylene glycol | 1.80- 5.00 | 26 | 1.06 -1.18 | |
| | Al ₂ O ₃ -ethylene glycol | 1.80- 5.00 | 60.4 | 1.10 -1.30 | |
| | Al ₂ O ₃ -ethylene glycol | 1.80- 5.00 | 302 | 1.08 -1.25 | |
| | Al ₂ O ₃ -pump oil | 5.00 | 60.4 | 1.39 | |
| | Al ₂ O ₃ -water | 5.00 | 60.4 | 1.23 | |
| Xie, et al. (2002b) | Al ₂ O ₃ -ethylene glycol | 5.00 | 60.4 | 1.29 | two-step method base fluid effect |
| | Al ₂ O ₃ -ethylene glycol | 5.00 | 60.4 | 1.38 | |
| | Al ₂ O ₃ -pump oil | 5.00 | 60.4 | 1.27 | |
| | Al ₂ O ₃ -glycerol | 5.00 | 60.4 | 1.27 | |
| | Al ₂ O ₃ -glycerol | 5.00 | 60.4 | 1.27 | |
| Xie, et al. (2002c) | Al ₂ O ₃ -water | 5.00 | 60.4 | 1.23 | two-step method base fluid effect |
| | Al ₂ O ₃ -ethylene glycol | 5.00 | 60.4 | 1.29 | |
| | Al ₂ O ₃ -pump oil | 5.00 | 60.4 | 1.38 | |
| | Al ₂ O ₃ -glycerol | 5.00 | 60.4 | 1.27 | |

| | | | | | |
|-----------------------|--|--|--|---|--|
| Das, et al. (2003a) | Al ₂ O ₃ -water (21°C) Al ₂ O ₃ -water (36°C) Al ₂ O ₃ -water (51°C) CuO-water (21°C) CuO-water (36°C) CuO-water (51°C) | 1.00- 4.00 1.00- 4.00 1.00- 4.00 1.00- 4.00 1.00- 4.00 1.00- 4.00 | 38.4 38.4 38.4 28.6 28.6 28.6 | 1.02 -1.09 1.07 -1.16 1.10 -1.24 1.07 -1.14 1.22 -1.26 1.29 -1.36 | two-step method temperature effect |
| Patel, et al. (2003) | citrate reduced Ag-water (30°C) citrate reduced Ag-water (60°C) citrate reduced Au-water (30°C) citrate reduced Au-water (60°C) citrate reduced Au-water (30°C) citrate reduced Au-water (60°C) thiolate covered Au-toluene (30°C) thiolate covered Au-toluene (60°C) thiolate covered Au-toluene (30°C) thiolate covered Au-toluene (60°C) thiolate covered Au-toluene (30°C) thiolate covered Au-toluene (60°C) | 0.001 0.001 0.00013 0.00013 0.00026 0.00026 0.005 0.005 0.008 0.008 0.011 0.011 | 60-70 60-70 10-20 10-20 10-20 10-20 3-4 3-4 3-4 3-4 3-4 3-4 | 1.030 1.04 1.03 1.05 1.05 1.08 1.03 1.05 1.06 1.07 1.06 1.09 | two-step method temperature effect |
| Xie, et al. (2003) | MWCNT-water MWCNT-ethylene glycol MWCNT (+ oleylamine)-decene | 0.40- 1.00 0.23- 1.00 0.25- 1.00 | 15x30000 15x30000 15x30000 | 1.03 -1.07 1.02 -1.13 1.04 -1.20 | two-step method nitric acid treatment |
| Assael, et al. (2004) | MWCNT (+ sodium dodecyl sulfate)-water | 0.60 | 100x>>50000 | 1.07 -1.38 | two-step method treatment effect dispersant concentration effect sonication time effect |
| Wen & Ding (2004a) | Al ₂ O ₃ (+ sodium dodecylbenzene sulfonate)-water | 0.19- 1.59 | 42 | 1.01 -1.10 | two-step method temperature effect |
| Wen & Ding (2004b) | MWCNT (+ sodium dodecyl benzene)-water (20°C) MWCNT (+ sodium dodecyl benzene)-water (45°C) | 0.04- 0.84 0.04- 0.84 | 20-60 (diameter) 20-60 (diameter) | 1.04 -1.24 1.05 -1.31 | two-step method temperature effect |
| Assael, et al. (2005) | DWCNT (+ hexadecyltrimethyl ammonium bromide)-water DWCNT (+ hexadecyltrimethyl ammonium bromide)-water MWCNT (+ hexadecyltrimethyl ammonium bromide)-water MWCNT (+ Nanospere AQ)-water | 0.75 1.00 0.60 0.60 | 5 (diameter) 5 (diameter) 130x>>10000 130x>>10000 | 1.03 1.08 1.34 1.28 | two-step method dispersant effect sonication time effect |
| Chon, et al. (2005) | Al ₂ O ₃ -water (21°C) Al ₂ O ₃ -water (71°C) Al ₂ O ₃ -water (21°C) Al ₂ O ₃ -water (71°C) Al ₂ O ₃ -water (21°C) Al ₂ O ₃ -water (71°C) Al ₂ O ₃ -water (21°C) Al ₂ O ₃ -water (71°C) | 1.00 1.00 1.00 1.00 1.00 1.00 4.00 4.00 | 11 11 47 47 150 150 47 47 | 1.09 1.15 1.03 1.10 1.004 1.09 1.08 1.29 | two-step method temperature effect |
| Hong, et al. (2005) | Fe-ethylene glycol | 0.20- 0.55 | 10 | 1.13 -1.18 | two-step method sonication time effect |
| Liu, et al. (2005) | MWCNT-ethylene glycol MWCNT (+ N-hydroxysuccinimide)-engine oil | 0.20- 1.00 1.00- 2.00 | 20-50 (diameter) 20-50 (diameter) | 1.02 -1.12 1.09 -1.30 | two-step method sonication time effect |

| | | | | | |
|---------------------------|--|--|--|--|---|
| Marquis & Chibante (2005) | SWCNT (+ dispersant)-diesel oil (Shell Rotella 15W-40) MWCNT (I) (+ succinimide)-polyalphaolefin (BP Amoco DS-166) MWCNT (II) (+ succinimide)-polyalphaolefin (BP Amoco DS-166) | 0.25- 1.00 0.25- 1.00 1.00 | (10- 50)×(0.3-10 μm) (20-300)×(1-100 μm) (20-300)×(1-100 μm) | 1.10 -1.46 1.30 -2.17 2.83 | two-step method treatment effect |
| Murshed, et al. (2005) | TiO ₂ (+ cetyltrimethylammoniumbromide)-water TiO ₂ (+ cetyltrimethylammoniumbromide)-water | 0.50- 5.00 0.50- 5.00 | 15 sphere 10×40 rod | 1.05 -1.30 1.08 -1.33 | two-step method |
| Wen & Ding (2005c) | Al ₂ O ₃ -water | 0.31- 0.72 | | 1.02 -1.06 | two-step method |
| Chopkar, et al. (2006) | Al ₇₀ Cu ₃₀ alloy-ethylene glycol | 0.19- 2.50 | 20-40 | 1.05 -2.25 | two-step method crystallite size effect |
| Ding, et al. (2006) | MWCNT (+ Gum Arabic)-water (20°C) MWCNT (+ Gum Arabic)-water (25°C) MWCNT (+ Gum Arabic)-water (30°C) | 0.05- 0.49 0.05- 0.49 0.05- 0.49 | | 1.00 -1.10 1.07 -1.27 1.18 -1.79 | two-step method temperature effect |
| Hong, et al. (2006) | Fe-ethylene glycol | 0.10- 0.55 | 10 (cluster) | 1.05 -1.18 | two-step method cluster size effect |
| Hwang, et al. (2006) | CuO-water SiO ₂ -water MWCNT-water CuO-ethylene glycol MWCNT-mineral oil | 1.00 1.00 1.00 1.00 0.50 | | 1.05 1.03 1.07 1.09 1.09 | two-step method |
| Kang, et al. (2006) | Ag-water SiO ₂ -water Diamond-ethylene glycol | 0.10- 0.39 1.00- 4.00 0.13- 1.33 | 8-15 15-20 30-50 | 1.03 -1.11 1.02 -1.05 1.03 -1.75 | two-step method |
| Lee, et al. (2006) | CuO-water (pH=3) CuO-water (pH=6) | 0.03- 0.30 0.03- 0.30 | 25 25 | 1.04 -1.12 1.02 -1.07 | two-step method pH value effect |
| Li & Peterson (2006) | Al ₂ O ₃ -water (27.5°C) Al ₂ O ₃ -water (32.5°C) Al ₂ O ₃ -water (34.7°C) CuO-water (28.9°C) CuO-water (31.3°C) CuO-water (33.4°C) | 2.00-10.00 2.00-10.00 2.00-10.00 2.00- 6.00 2.00- 6.00 2.00- 6.00 | 36 36 36 29 29 29 | 1.08 -1.11 1.15 -1.22 1.18 -1.29 1.35 -1.36 1.35 -1.50 1.38 -1.51 | two-step method temperature effect |
| Liu, et al. (2006) | Cu-water Cu-water Cu-water Cu-water Cu-water Cu-water Cu-water Cu-water | 0.05 0.10 0.10 0.05 0.10 0.05 0.20 0.20 0.20 | | 1.04 1.24 1.24 1.12 1.11 1.09 1.10 1.04 1.13 | one-step chemical method settlement time effect |
| Putnam, et al. (2006) | 11-mercapto-1-undecanol functionalized Au (+ alkanethiolate)-ethanol dodecanethiol functionalized Au (+ alkanethiolate)-toluene C ₆₀ -C ₇₀ fullerene-toluene | 0.01- 0.07 0.11- 0.36 0.15- 0.60 | 4 2 | 1.003-1.013 1.000-1.015 1.002-1.009 | two-step method |
| Wen & Ding (2006) | TiO ₂ -water (pH=3) | 0.29- 0.68 | 34 | 1.02 -1.06 | two-step method dispersant HNO ₃ & NaOH |

| Yang, et al. (2006) | MWCNT (+ polyisobutene succinimide)-polyalphaolefin | 0.04- 0.34 | | 1.06 -3.00 | two-step method dispersing energy effect aspect ratio effect dispersant concentration effect |
|---------------------|---|------------|--------|------------|---|
| Yang & Han (2006) | Bi ₂ Te ₃ - hexadecane oil (20°C) | 0.80 | 20×170 | 1.06 | two-step method surfactant |
| | Bi ₂ Te ₃ - hexadecane oil (50°C) | 0.80 | 20×170 | 1.04 | |
| | Bi ₂ Te ₃ -perfluoro- <i>n</i> -hexane (3°C) | 0.80 | 20×170 | 1.08 | |
| | Bi ₂ Te ₃ -perfluoro- <i>n</i> -hexane (50°C) | 0.80 | 20×170 | 1.06 | |

Table 2. Single-Phase Heat Transfer Enhancements

| Author (Year) | Nanofluid | Concentration (vol %) | Particle Size (nm) | Enhancement (ratio) | Note |
|---------------------------|--|-----------------------|--------------------|---------------------|--|
| Pak & Cho (1998) | Al ₂ O ₃ -water (pH=3) | 1.34 | 13 | 1.07 -1.30 | two-step method |
| | Al ₂ O ₃ -water (pH=3) | 2.78 | 13 | 1.24 -1.35 | 10.66-mm stainless steel tube |
| | TiO ₂ -water (pH=10) | 0.99 | 27 | 0.93 -1.09 | turbulent flow |
| | TiO ₂ -water (pH=10) | 2.04 | 27 | 0.98 -1.16 | enhanced Nusselt number |
| | TiO ₂ -water (pH=10) | 3.16 | 27 | 1.07 -1.20 | Re=10000-100000 |
| Putra, et al. (2003) | Al ₂ O ₃ -water (L/D=0.5) | 1.00 | 131.2 | 0.85 -1.02 | two-step method |
| | Al ₂ O ₃ -water (L/D=1.0) | 1.00 | 131.2 | 0.87 -1.04 | horizontal cylinder |
| | Al ₂ O ₃ -water (L/D=0.5) | 4.00 | 131.2 | 0.70 -0.85 | natural convection |
| | Al ₂ O ₃ -water (L/D=1.0) | 4.00 | 131.2 | 0.63 -0.82 | cylinder aspect ratio L/D effect |
| | Al ₂ O ₃ -water (L/D=1.5) | 4.00 | 131.2 | 0.75 -0.85 | reduced Nusselt number |
| | CuO-water (L/D=1.0) | 1.00 | 87.3 | 0.79 -0.93 | Ra=2450000-31500000 |
| | CuO-water (L/D=1.0) | 4.00 | 87.3 | 0.54 -0.67 | |
| Xuan & Li (2003) | Cu-water | 0.30 | <100 | 0.99 -1.05 | two-step method |
| | Cu-water | 0.50 | <100 | 1.01 -1.08 | 10-mm brass tube |
| | Cu-water | 0.80 | <100 | 1.07 -1.13 | turbulent flow |
| | Cu-water | 1.00 | <100 | 1.13 -1.15 | enhanced Nusselt number |
| | Cu-water | 1.20 | <100 | 1.14 -1.21 | Re=9800-23600 |
| | Cu-water | 1.50 | <100 | 1.23 -1.27 | |
| | Cu-water | 2.00 | <100 | 1.25 -1.35 | |
| | | | | | |
| Faulkner, et al. (2004) | MWCNT (+ sodium dodecylbenzene sulfonate)-water (q''=0.1 W/cm ²) | 1.10 | | 1.01 -4.69 | two-step method |
| | MWCNT (+ sodium dodecylbenzene sulfonate)-water (q''=0.5 W/cm ²) | 1.10 | | 0.48 -1.99 | D _h =355 μm microchannel |
| | MWCNT (+ sodium dodecylbenzene sulfonate)-water (q''=0.1 W/cm ²) | 2.20 | | 1.93 -2.21 | laminar flow |
| | MWCNT (+ sodium dodecylbenzene sulfonate)-water (q''=0.5 W/cm ²) | 2.20 | | 1.17 -1.63 | heat flux effect |
| | MWCNT (+ sodium dodecylbenzene sulfonate)-water (q''=0.1 W/cm ²) | 4.40 | | 1.20 -1.71 | enhanced heat transfer coefficient |
| | MWCNT (+ sodium dodecylbenzene sulfonate)-water (q''=0.5 W/cm ²) | 4.40 | | 0.90 -1.19 | Re=2-17 |
| | MWCNT (+ Nanospense AQ)-water (q''=0.1 W/cm ²) | 4.40 | | 0.86 -1.51 | |
| | MWCNT (+ Nanospense AQ)-water (q''=0.5 W/cm ²) | 4.40 | | 0.81 -1.08 | |
| | | | | | |
| | | | | | |
| Wen & Ding (2004a) | Al ₂ O ₃ (+ sodium dodecylbenzene sulfonate)-water (x/D=63) | 0.60 | 42 | 1.04 -1.12 | two-step method |
| | Al ₂ O ₃ (+ sodium dodecylbenzene sulfonate)-water (x/D=63) | 1.00 | 42 | 1.09 -1.22 | 4.5-mm copper tube |
| | Al ₂ O ₃ (+ sodium dodecylbenzene sulfonate)-water (x/D=63) | 1.60 | 42 | 1.25 -1.38 | laminar flow |
| | Al ₂ O ₃ (+ sodium dodecylbenzene sulfonate)-water (x/D=116) | 0.60 | 42 | 1.10 -1.20 | axial distance effect |
| | Al ₂ O ₃ (+ sodium dodecylbenzene sulfonate)-water (x/D=116) | 1.00 | 42 | 1.12 -1.20 | enhanced Nusselt number |
| | Al ₂ O ₃ (+ sodium dodecylbenzene sulfonate)-water (x/D=116) | 1.60 | 42 | 1.26 -1.35 | Re=710-1940 axial distance/diameter effect |
| Wen & Ding (2005c & 2006) | TiO ₂ (electrostatic repulsion)-water (pH=3) | 0.19 | 34 | 0.85 -0.98 | two-step method |
| | TiO ₂ (electrostatic repulsion)-water (pH=3) | 0.35 | 34 | 0.77 -0.95 | dispersant HNO ₃ & NaOH |
| | TiO ₂ (electrostatic repulsion)-water (pH=3) | 0.57 | 34 | 0.64 -0.87 | short vertical cylinder natural convection reduced Nusselt number Ra=23000-224000 |

| | | | | | |
|-----------------------|--|--|---|--|--|
| Yang, et al. (2005) | graphite-transmission fluid (50°C) graphite-transmission fluid (70°C) graphite-transmission fluid (50°C) graphite-transmission fluid (70°C) graphite-mixture of two synthetic base oils (50°C) graphite-mixture of two synthetic base oils (70°C) graphite-mixture of two synthetic base oils (50°C) graphite-mixture of two synthetic base oils (70°C) | 0.77 | 1000-2000×20-40 | 0.97 -1.02 | two-step method 4.57-mm smooth tube laminar flow temperature effect enhanced heat transfer coefficient Re=5-104 |
| Ding, et al. (2006) | MWCNT (+ 0.25 wt % Gum Arabic)-water (x/D=26.2) MWCNT (+ 0.25 wt % Gum Arabic)-water (x/D=63.3) MWCNT (+ 0.25 wt % Gum Arabic)-water (x/D=116.4) MWCNT (+ 0.25 wt % Gum Arabic)-water (x/D=147.1) MWCNT (+ 0.25 wt % Gum Arabic)-water (x/D=173.8) | 0.048 | | 1.63 -1.93 1.96 -2.27 1.63 -2.28 1.49 -2.65 1.33 -2.53 | two-step method 4.5-mm copper tube laminar flow axial distance effect enhanced heat transfer coefficient Re=800-1200 |
| Harris, et al. (2006) | Al ₂ O ₃ -water Al ₂ O ₃ -water Al ₂ O ₃ -water Al ₂ O ₃ -water Al ₂ O ₃ -water CuO-water CuO-water CuO-water CuO-water | 0.20 1.00 2.00 2.50 3.00 0.20 1.00 2.00 2.50 3.00 | 20 20 20 20 20 50-60 50-60 50-60 50-60 50-60 | 1.04 -1.10 1.12 -1.19 1.13 -1.31 1.12 -1.38 1.08 -1.41 1.02 -1.11 1.06 -1.20 1.03 -1.27 1.02 -1.36 1.02 -1.38 | two-step method 6-mm copper tube laminar flow constant wall temperature enhanced Nusselt number Re=650-2050 Pe=2400-6800 |

Table 3. Pool-Boiling Heat Transfer Enhancements

| Author (Year) | Nanofluid | Concentration (vol %) | Particle Size (nm) | Enhancement (ratio) | Note |
|---------------------|--|-----------------------|--------------------|---------------------|--|
| Das, et al. (2003b) | Al ₂ O ₃ -water (smooth cylindrical surface) | 1.00 | 38 | 0.72 -0.80 | two-step method reduced Nusselt number Re=0.44-2.89 |
| | Al ₂ O ₃ -water (smooth cylindrical surface) | 2.00 | 38 | 0.69 -0.76 | |
| | Al ₂ O ₃ -water (smooth cylindrical surface) | 4.00 | 38 | 0.60 -0.65 | |
| | Al ₂ O ₃ -water (rough cylindrical surface) | 1.00 | 38 | 0.65 -0.69 | |
| | Al ₂ O ₃ -water (rough cylindrical surface) | 2.00 | 38 | 0.64 -0.69 | |
| | Al ₂ O ₃ -water (rough cylindrical surface) | 4.00 | 38 | 0.57 -0.60 | |
| Das, et al. (2003c) | Al ₂ O ₃ -water (4 mm tube) | 1.00 | 58.4 | 0.79 -0.85 | two-step method reduced Nusselt number Re=0.09-2.92 |
| | Al ₂ O ₃ -water (6.5 mm tube) | 1.00 | 58.4 | 0.71 -0.79 | |
| | Al ₂ O ₃ -water (20 mm tube) | 1.00 | 58.4 | 0.83 -0.85 | |
| | Al ₂ O ₃ -water (4 mm tube) | 4.00 | 58.4 | 0.46 -0.55 | |
| | Al ₂ O ₃ -water (6.5 mm tube) | 4.00 | 58.4 | 0.64 -0.71 | |
| | Al ₂ O ₃ -water (20 mm tube) | 4.00 | 58.4 | 0.64 -0.70 | |
| Bang & Chang (2005) | Al ₂ O ₃ -water (horizontal surface) | 0.50 | 47 | 0.75 -0.92 | two-step method reduced heat transfer coefficient heat flux=5000-505.50 (kW/m ²) |
| | Al ₂ O ₃ -water (horizontal surface) | 1.00 | 47 | 0.78 -0.89 | |
| | Al ₂ O ₃ -water (horizontal surface) | 2.00 | 47 | 0.70 -0.83 | |
| | Al ₂ O ₃ -water (horizontal surface) | 4.00 | 47 | 0.68 -0.83 | |
| Wen & Ding (2005b) | Al ₂ O ₃ -water (horizontal surface) | 0.08 | 10-50 | 1.06 -1.22 | two-step method enhanced heat transfer coefficient heat flux=26.50-126.00 (kW/m ²) |
| | Al ₂ O ₃ -water (horizontal surface) | 0.18 | 10-50 | 1.12 -1.29 | |
| | Al ₂ O ₃ -water (horizontal surface) | 0.24 | 10-50 | 1.19 -1.36 | |
| | Al ₂ O ₃ -water (horizontal surface) | 0.32 | 10-50 | 1.24 -1.40 | |

Table 4. Pool-Boiling Critical Heat Flux Enhancements

| Author (Year) | Nanofluid | Concentration (vol %) | Particle Size (nm) | Enhancement (ratio) | Note |
|-------------------------|--|-----------------------|--------------------|---------------------|--|
| You, et al. (2003) | Al ₂ O ₃ -water (horizontal surface) | 0.00- 0.13 % | | 1.24 -3.11 | two-step method |
| Vassallo, et al. (2004) | SiO ₂ -water (horizontal NiCr wire) | 0.50 | 15 | 1.60 | two-step method |
| | SiO ₂ -water (horizontal NiCr wire) | 0.50 | 50 | 3.00 | |
| | SiO ₂ -water (horizontal NiCr wire) | 0.50 | 3000 | 1.50 | |
| Bang & Chang (2005) | Al ₂ O ₃ -water (horizontal surface) | 0.50- 4.00 | 47 | 1.32 -1.52 | two-step method |
| | Al ₂ O ₃ -water (vertical surface) | 0.50- 4.00 | 47 | 1.13 | |
| Milanova & Kumar (2005) | SiO ₂ -water (horizontal NiCr wire, pH=10.2) | 0.5 | 10 | 4.52 (water pH=7) | two-step method ion effect pH value effect |
| | SiO ₂ -water (horizontal NiCr wire, pH=9.22) | 0.5 | 20 | 2.39 (water pH=7) | |
| | SiO ₂ -buffer (horizontal NiCr wire, pH=10) | 0.5 | 10 | 3.16 | |
| | SiO ₂ -buffer (horizontal NiCr wire, pH=10) | 0.5 | 20 | 2.30 | |
| Liu & Qiu (2006) | CuO-water (saturated, jet on horizontal surface) | 0.02- 0.32 | 50 | 1.17 -1.25 | two-step method |
| | CuO-water (subcooled, jet on horizontal surface) | 0.02- 0.32 | 50 | 1.16 -1.25 | |

Appendix B.

Mathematical Models of Nanofluids

Table 5. Models of Effective Thermal Conductivity

| | |
|---|---|
| Maxwell 1873 (spheres) | $k_e = k_m + 3v_p \frac{k_p - k_m}{2k_m + k_p - v_p(k_p - k_m)} k_m$ |
| Rayleigh 1892 (spheres, simple cubic arrays) | $k_e = k_m + 3v_p \frac{k_p - k_m}{2k_m + k_p - v_p \left(1 + 3.939v_p^{7/3} \frac{k_p - k_m}{4k_m + 3k_p} \right) (k_p - k_m)} k_m$ |
| Wiener 1912 (arbitrary particles) | $k_e = k_m + (u + 1)v_p \frac{k_p - k_m}{uk_m + k_p - v_p(k_p - k_m)} k_m, \quad 0 \leq u \leq \infty$ |
| Fricke 1924; Fricke 1953 (ellipsoids) | $k_e = k_m + \frac{1}{3}v_p \sum_{i=a,b,c} \frac{k_p - k_m}{k_m + d_{pi}(k_p - k_m)} k_m$ |
| Bruggeman 1935 (spheres) | $1 - v_p = \frac{k_p - k_e}{k_p - k_m} \left(\frac{k_m}{k_e} \right)^{1/3}$ |
| Bruggeman 1935; Böttcher 1945; Landauer 1952 (spheres) | $(1 - v_p) \frac{k_m - k_e}{2k_e + k_m} + v_p \frac{k_p - k_e}{2k_e + k_p} = 0$ |
| Polder and van Santen 1946; Taylor 1965; Taylor 1966 (ellipsoids) | $k_e = k_m + \frac{1}{3}v_p \sum_{i=a,b,c} \frac{k_p - k_m}{k_e + d_{pi}(k_p - k_e)} k_e$ |
| Kemer 1956; Pauly and Schwan 1959; Schwan, et al. 1962; Lamb, et al. 1978; Benveniste and Miloh 1991; Yu and Choi 2003; Wang, et al. 2003 (spheres with shells) | $k_e = k_m + 3v_c \frac{k_c - k_m}{2k_m + k_c - v_c(k_c - k_m)} k_m$ |
| Van de Hulst 1957; Lu and Song 1996; Xue 2000 (spheres with shells) | $(1 - v_c) \frac{k_m - k_e}{2k_e + k_m} + v_c \frac{k_c - k_e}{2k_e + k_c} = 0$ |
| Hamilton and Crosser 1962 (arbitrary particles) | $k_e = k_m + 3\Psi^{-1}v_p \frac{k_p - k_m}{(3\Psi^{-1} - 1)k_m + k_p - v_p(k_p - k_m)} k_m$ |
| Jeffrey 1973 (spheres) | $k_e = k_m + 3v_p \left[1 + v_p \frac{\sigma_1(2k_m + k_p) + (k_p - k_m)}{2k_m + k_p} \right] \frac{k_p - k_m}{2k_m + k_p} k_m$ |
| Granqvist and Hunderi 1977; Granqvist and Hunderi 1978 (ellipsoids) | $(1 - v_p) \frac{k_m - k_e}{2k_e + k_m} + \frac{1}{9}v_p \sum_{i=a,b,c} \frac{k_p - k_e}{k_e + d_{pi}(k_p - k_e)} = 0$ |
| Landauer 1978 (spheres) | $(1 - v_s - v_p) \frac{k_m - k_e}{2k_e + k_m} + v_s \frac{k_s - k_e}{2k_e + k_s} + v_p \frac{k_p - k_e}{2k_e + k_p} = 0$ |
| Davis 1986 (spheres) | $k_e = k_m + 3v_p(1 + v_p\sigma_1) \frac{k_p - k_m}{2k_m + k_p - v_p(k_p - k_m)} k_m$ |
| Benveniste 1987; Hasselman and Johnson 1987 (spheres with contact resistance) | $k_e = k_m + 3v_p \frac{k_p^R - k_m}{2k_m + k_p^R - v_p(k_p^R - k_m)} k_m$ |

| |
|--|
| <p>Xue 2000 (ellipsoids)</p> $(1 - v_p) \sum_{i=a,b,c} \frac{k_m - k_e}{k_e + d_{mi}(k_m - k_e)} + v_p \sum_{i=a,b,c} \frac{k_p - k_e}{k_e + d_{pi}(k_p - k_e)} = 0$ |
| <p>Nan, et al. 2003 (carbon nanotubes)</p> $k_e = k_m + \frac{1}{3} v_p k_p$ |
| <p>Wang, et al. 2003 (spheres)</p> $k_e = k_m + \frac{3v_p \int_0^\infty \frac{k_p(r) - k_m}{2k_m + k_p(r)} n(r) dr}{(1 - v_p) + 3v_p \int_0^\infty \frac{k_m}{2k_m + k_p(r)} n(r) dr} k_m, \text{ where } n(r) = \frac{1}{\sqrt{2\pi}(\ln \sigma)r} e^{-[\ln(r/r_p)/(\sqrt{2\pi} \ln \sigma)]^2} \text{ and } \sigma = 1.5.$ |
| <p>Xuan, et al. 2003 (spheres with Brownian motion and cluster effect)</p> $k_e = k_m + 3v_p \frac{k_p - k_m}{2k_m + k_p - v_p(k_p - k_m)} k_m + \frac{1}{2} \rho_p C_{pp} v_p \sqrt{\frac{k_B T}{3\pi\mu_m r_c}}$ |
| <p>Jang and Choi 2004, (spheres)</p> $k_e = (1 - v_p)k_m + v_p k_p + 3c(r_m/r_p)v_p \left(\frac{k_B T}{3\pi\mu_m v_m l_m} \right)^2 \text{Pr} k_m, \text{ where } c \text{ is an empirical parameter.}$ |
| <p>Koo and Kleinstreuer 2004 (spheres with Brownian motion effect for CuO based nanofluids)</p> $k_e = k_m + 3v_p \frac{k_p - k_m}{2k_m + k_p - v_p(k_p - k_m)} k_m + 5 \times 10^4 \beta \rho_m C_{pm} v_p \sqrt{\frac{k_B T}{2\rho_p r_p}} [(-134.63 + 1722.3v_p) + (0.4705 - 6.04v_p)T],$ <p>where the particle motion related empirical parameter $\beta = \begin{cases} 0.0137(100v_p)^{-0.8229} & v_p < 0.01 \\ 0.0011(100v_p)^{-0.7272} & v_p > 0.01 \end{cases}$</p> |
| <p>Kumar, et al. 2004 (spheres)</p> $k_e = k_m + c \left(\frac{r_m}{r_p} \right) \left(\frac{v_p}{1 - v_p} \right) \left(\frac{k_B T}{2\pi\mu_m r_p^2} \right), \text{ where } c \text{ is an empirical parameter.}$ |
| <p>Nan, et al. 2004 (carbon nanotubes with contact resistance)</p> $k_e = k_m + \frac{1}{3} v_p \frac{k_p}{1 + Rk_p/a}$ |
| <p>Yu and Choi 2004 (ellipsoids with shell)</p> $k_e = k_m + \Psi^{-1} v_c \sum_{a,b,c} \frac{k_{ci} - k_m}{(3\Psi^{-1} - 1)k_m + k_{ci} - v_c(k_{ci} - k_m)} k_m$ |
| <p>Prasher, et al. 2005; Prasher, et al. 2006a (spheres with contact resistance and Brownian motion effect)</p> $k_e = \left[1 + c v_p \left(\frac{9k_B T}{\pi\rho_p v_m^2 r_p} \right)^m \text{Pr}^{0.333} \right] \left\{ k_m + 3v_p \frac{k_p^R}{2k_m + k_p^R - v_p(k_p^R - k_m)} k_m \right\}, \text{ where } c \text{ and } m \text{ are empirical parameters.}$ |
| <p>Xue 2005 (carbon nanotubes)</p> $k_e = k_m + \frac{\frac{4}{\pi} v_p \frac{k_p - k_m}{\sqrt{k_m k_p}} \arctan \sqrt{\frac{k_p}{k_m}}}{(1 - v_p) + \frac{4}{\pi} v_p \frac{k_m}{\sqrt{k_m k_p}} \arctan \sqrt{\frac{k_p}{k_m}}} k_m \qquad k_e = k_m + \frac{2v_p \ln \left(\frac{k_p + k_m}{2k_m} \right)}{(1 - v_p) + 2v_p \frac{k_m}{k_p - k_m} \ln \left(\frac{k_p + k_m}{2k_m} \right)} k_m$ |
| <p>Yu and Choi 2005 (spheres with shells, simple cubic arrays)</p> $k_e = \left\{ 1 - \sqrt[3]{\frac{3v_c}{4\pi}} \left[2 - \frac{\sqrt[3]{16/(9\pi v_c^2)} k_m}{k_1 k_2} \ln \frac{(k_2 + k_1)(k_2 - \sqrt[3]{v_r} k_1)}{(k_2 - k_1)(k_2 + \sqrt[3]{v_r} k_1)} + \frac{\sqrt[3]{16/(9\pi v_c^2)} k_m}{k_3 k_4} \ln \frac{k_4 + \sqrt[3]{v_r} k_3}{k_4 - \sqrt[3]{v_r} k_3} \right] \right\}^{-1} k_m,$ <p>where $k_1 = \sqrt{k_s - k_m}$, $k_2 = \sqrt[3]{16/(9\pi v_c^2)} k_m + (k_s - k_m)$, $k_3 = \sqrt{k_p - k_m}$, and $k_4 = \sqrt[3]{16/(9\pi v_c^2)} k_m + (k_s - k_m) + \sqrt[3]{v_r^2} (k_p - k_s)$</p> |

Prasher, et al. 2006b (spheres with aggregate effect)

$$k_e = k_m + 3(r_a/r_p)^{3-d_f} v_p \frac{k_a - k_m}{2k_m + k_a - (r_a/r_p)^{3-d_f} v_p (k_a - k_m)} k_m,$$

where $\left[1 - (r_p/r_a)^{3-d_f}\right] \frac{k_m - k_a}{2k_a + k_m} + (r_p/r_a)^{3-d_f} \frac{k_p - k_a}{2k_a + k_p} = 0$ and $1.75 \leq d_f \leq 2.5$.

Table 6. Models of Effective Viscosity

| | |
|---|--|
| Einstein 1906 (spheres) | $\mu_e = (1 + 2.5v_p)\mu_m$ |
| Simha 1940 (prolate spheroids, $a \gg b = c$) | $\mu_e = \left\{ 1 + \frac{1}{15} \left[14 + \frac{(a/c)^2}{\ln(2a/c) - 1.5} + \frac{3(a/c)^2}{\ln(2a/c) - 0.5} \right] v_p \right\} \mu_m$ |
| Simha 1940 (oblate spheroids, $a = b \gg c$) | $\mu_e = \left[1 + \frac{16}{15} \frac{(a/c)}{\arctan(a/c)} v_p \right] \mu_m$ |
| Eilers 1941 (spheres, $0.5236 \leq v_{p \max} \leq 0.7405$) | $\mu_e = \left[1 + \frac{1.25}{1 - (v_p/v_{p \max})} v_p \right]^2 \mu_m = \left\{ 1 + 2.5v_p + [1.5625 + (2.5/v_{p \max})]v_p^2 + \dots \right\} \mu_m$ |
| De Bruijn 1942 (spheres) | $\mu_e = \frac{1}{1 - 2.5v_p + 1.552v_p^2} \mu_m = (1 + 2.5v_p + 4.698v_p^2 + \dots)\mu_m$ |
| Kuhn and Kuhn 1945 (prolate spheroids, $a \gg b = c$) | $\mu_e = \left\{ 1 + \frac{1}{15} \left[24 + \frac{(a/c)^2}{\ln(2a/c) - 1.5} + \frac{3(a/c)^2}{\ln(2a/c) - 0.5} \right] v_p \right\} \mu_m$ |
| Vand 1948 (spheres) | $\mu_e = (1 + 2.5v_p + 7.349v_p^2 + \dots)\mu_m$ |
| Vand 1948 (spheres) | $\mu_e = e^{2.5v_p} \mu_m = (1 + 2.5v_p + 3.125v_p^2 + \dots)\mu_m$ |
| Robinson 1949 (arbitrary particles) | $\mu_e = \left(1 + \frac{c_p v_p}{1 - s_r v_p} \right) \mu_m = (1 + c_p v_p + c_p s_r v_p^2 + \dots)\mu_m$ |
| Saitō 1950 (spheres) | $\mu_e = \left(1 + \frac{2.5}{1 - v_p} v_p \right) \mu_m = (1 + 2.5v_p + 2.5v_p^2 + \dots)\mu_m$ |
| Mooney 1951 (spheres, $0.5236 \leq v_{p \max} \leq 0.7405$) | $\mu_e = e^{2.5v_p / [1 - (v_p/v_{p \max})]} \mu_m = \left\{ 1 + 2.5v_p + [3.125 + (2.5/v_{p \max})]v_p^2 + \dots \right\} \mu_m$ |
| Brinkman 1952; Roscoe 1952 (spheres) | $\mu_e = \frac{1}{(1 - v_p)^{2.5}} \mu_m = (1 + 2.5v_p + 4.375v_p^2 + \dots)\mu_m$ |
| Simha 1952 (spheres, $0.5236 \leq v_{p \max} \leq 0.7405$) | $\mu_e = \left\{ 1 + 2.5v_p + [125/(64v_{p \max})]v_p^2 + \dots \right\} \mu_m$ |
| Eshelby 1957 (ellipsoids) | $\mu_e = \left(1 + \frac{15}{2} \frac{1 - \sigma_p}{4 - 5\sigma_p} v_p \right) \mu_m = \left(1 + \frac{15}{7} v_p \right) \mu_m, \text{ where the Poisson's ratio } \sigma_p \approx 1/3.$ |
| Frankel and Acrivos 1967 (spheres, $0.5236 \leq v_{p \max} \leq 0.7405$) | $\mu_e = \frac{9}{8} \frac{(v_p/v_{p \max})^{1/3}}{1 - (v_p/v_{p \max})^{1/3}} \mu_m$ |
| Batchelor 1977 (spheres) | $\mu_e = (1 + 2.5v_p + 6.2v_p^2)\mu_m$ |

| |
|--|
| <p>Krieger 1972 (spheres, $0.5236 \leq v_{p \max} \leq 0.7405$)</p> $\mu_e = \frac{1}{[1 - (v_p/v_{p \max})]^{1.82}} \mu_m = [1 + (1.82/v_{p \max})v_p + (2.5662/v_{p \max}^2)v_p^2 + \dots] \mu_m$ |
| <p>Lundgren 1972 (spheres)</p> $\mu_e = \frac{1}{1 - 2.5v_p} \mu_m = (1 + 2.5v_p + 6.25v_p^2 + \dots) \mu_m$ |
| <p>Graham 1981 (spheres, $0.5236 \leq v_{p \max} \leq 0.7405$)</p> $\mu_e = \left[1 + 2.5v_p + \frac{4.5}{(s_p/r_p)[2 + (s_p/r_p)][1 + (s_p/r_p)]^2} \right] \mu_m,$ <p>where, for a simple cubic packing, the interparticle spacing $s_p = 2[1 - (v_p/v_{p \max})^{1/3}][v_p/v_{p \max}]^{-1/3}r_p$.</p> |
| <p>Phan-Thien and Graham 1991 (fibers, $a > b = c$, $5 < a/c < 25$, $0.5236 \leq v_{p \max} \leq 0.7405$)</p> $\mu_e = \left\{ 1 + [1.461 + 0.138(a/c)] \frac{1 - 0.5(v_p/v_{p \max})}{[1 - (v_p/v_{p \max})]^2} v_p \right\} \mu_m = \left\{ 1 + [1.461 + 0.138(a/c)]v_p + [1.461 + 0.138(a/c)][1.5/v_{p \max}]v_p^2 + \dots \right\} \mu_m$ |
| <p>Liu and Masliyah 1996 (spheres, $0.5236 \leq v_{p \max} \leq 0.7405$)</p> $\mu_e = \left\{ \frac{1}{[1 - (v_p/v_{p \max})]^2} + [c_1 - (2/v_{p \max})]v_p + [c_2 - (6/v_{p \max}^2)]v_p^2 \right\} \mu_m = \left\{ 1 + c_1v_p + [c_2 - (3/v_{p \max}^2)]v_p^2 + \dots \right\} \mu_m$ |
| <p>Tseng and Lin 2003 (for TiO₂-in-water nanofluids)</p> $\mu_e = 13.47e^{35.98v_p} \mu_m$ |
| <p>Maïga, et al. 2004 (for Al₂O₃-in-water nanofluids)</p> $\mu_e = (1 + 7.3v_p + 123v_p^2) \mu_m$ |
| <p>Maïga, et al. 2004 (for Al₂O₃-in-ethylene glycol nanofluids)</p> $\mu_e = (1 - 0.19v_p + 306v_p^2) \mu_m$ |
| <p>Koo and Kleinstreuer 2005 (additional viscosity for CuO based nanofluids from Brownian motion)</p> $\mu_{Brownian} = 5 \times 10^4 \beta \rho_m v_p \sqrt{\frac{k_B T}{2 \rho_p r_p}} [(-134.63 + 1722.3v_p) + (0.4705 - 6.04v_p)T],$ <p>where the particle motion related empirical parameter $\beta = \begin{cases} 0.0137(100v_p)^{-0.8229} & v_p < 0.01 \\ 0.0011(100v_p)^{-0.7272} & v_p > 0.01 \end{cases}$.</p> |
| <p>Kulkarni, et al. 2006 (for CuO-in-water nanofluids)</p> $\ln \mu_e = -(2.8751 + 53.548v_p - 107.12v_p^2) + (1078.3 + 15857v_p + 20587v_p^2)(1/T)$ |

Table 7. Models of Effective Heat Transfer Coefficient

| |
|---|
| Pak and Cho 1998 (for Al ₂ O ₃ -in-water and TiO ₂ -in-water nanofluids, turbulent flow) $\text{Nu} = 0.021 \text{Re}^{0.8} \text{Pr}^{0.5}$ |
| Das, et al. 2003b (for Al ₂ O ₃ -in-water nanofluids, pool boiling) $\text{Nu} = c \text{Re}_p^m \text{Pr}^{0.4}$, where c and m are particle volume concentration dependent parameters. |
| Xuan and Li 2003 (for CuO-in-water nanofluids, turbulent flow) $\text{Nu} = 0.0059(1.0 + 7.6286v_p^{0.6886} \text{Pe}_p^{0.001}) \text{Re}^{0.9238} \text{Pr}^{0.4}$ |
| Yang, et al. 2005 (for graphite-in-transmission fluid and graphite-in-synthetic oil mixture nanofluids, laminar flow) $\text{Nu} = c \text{Re}^m \text{Pr}^{1/3} (D/L)^{1/3} (\mu_b/\mu_w)^{0.14}$, where c and m are nanofluid and temperature dependent empirical parameters. |
| Buongiorno 2006 (turbulent) $\text{Nu} = \frac{(f/8)(\text{Re}-1000) \text{Pr}}{1 + \delta_v^+ (f/8)^{1/2} (\text{Pr}_v^{2/3} - 1)}$, where the dimensionless thickness of the laminar sublayer δ_v^+ is an empirical parameter. |

References

- Ali, A., K. Vafai, and A.-R. A. Khaled (2003). Comparative Study between Parallel and Counter Flow Configurations between Air and Falling Film Desiccant in the Presence of Nanoparticle Suspensions. *International Journal of Energy Research* 27: 725-745.
- Ali, A., K. Vafai, and A.-R. A. Khaled (2004). Analysis of Heat and Mass Transfer between Air and Falling Film in a Cross Flow Configuration. *International Journal of Heat and Mass Transfer* 47: 743-755.
- Assael, M. J., C.-F. Chen, I. Metaxa, and W. A. Wakeham (2004). Thermal Conductivity of Suspensions of Carbon Nanotubes in Water. *International Journal of Thermophysics* 25: 971-985.
- Assael, M. J., I. N. Metaxa, J. Arvanitidis, D. Christofilos, and C. Lioutas (2005). Thermal Conductivity Enhancement in Aqueous Suspensions of Carbon Multi-Walled and Double-Walled Nanotubes in the Present of Two Different Dispersants. *International Journal of Thermophysics* 26: 647-664.
- Bang, I. C., and S. H. Chang (2005). Boiling Heat Transfer Performance and Phenomena of Al_2O_3 -Water Nano-Fluids from a Plain Surface in a Pool. *International Journal of Heat and Mass Transfer* 48: 2407-2419.
- Batchelor, G. K. (1977). The Effect of Brownian Motion on the Bulk Stress in a Suspension of Spherical Particles. *Journal of Fluid Mechanics* 83: 97-117.
- Benveniste, Y. (1987). Effective Thermal Conductivity of Composites with a Thermal Contact Resistance between the Constituents: Nondilute Case. *Journal of Applied Physics* 61: 2840-2843.
- Benveniste, Y., and T. Miloh (1991). On the Effective Thermal Conductivity of Coated Short-Fiber Composites. *Journal of Applied Physics* 69: 1337-1344.
- Bhattacharya, P., S. K. Saha, A. Yadav, P. E. Phelan, and R. S. Prasher (2004). Brownian Dynamics Simulation to Determine the Effect Thermal Conductivity of Nanofluids. *Journal of Applied Physics* 95: 6492-6494.
- Bilboul, R. R. (1969). A Note on the Permittivity of a Double-Layer Ellipsoid. *British Journal of Applied Physics (Series 2)* 2: 921-923.
- Böttcher, C. J. F. (1945). The Dielectric Constant of Crystalline Powders. *Recueil des Travaux Chimiques des Pays-Bas* 64: 47-51.
- Brinkman, H. C. (1952). The Viscosity of Concentrated Suspensions and Solutions. *The Journal of Chemical Physics* 20: 571.

Bruggeman, D. A. G. (1935). Berechnung verschiedener physikalischer Konstanten von heterogenen Substanzen: I. Dielektrizitätskonstanten und Leitfähigkeiten der Mischkörper aus isotropen Substanzen, *Annalen der Physik* 24: 636-664.

Buongiorno, J. (2006). Convective Transport in Nanofluids. *Transactions of the ASME, Journal of Heat Transfer* 128: 240-250.

Cao, H. L., X. F. Qian, Q. Gong, W. M. Du, X. D. Ma, and Z. K. Zhu (2006). Shape- and Size-Controlled Synthesis of Nanometer ZnO from a Simple Solution Route at Room Temperature. *Nanotechnology* 17: 3632-3636.

Cao, Q., and J. Tavares (2006). Dual-Plasma Synthesis of Coated Nanoparticles and Nanofluids. <http://aiche.confex.com/aiche/2006/techprogram/P65561.HTM>.

Chang, H., T. T. Tsung, L. C. Chen, Y. C. Yang, H. M. Lin, C. K. Lin, and C. S. Jwo (2005). Nanoparticle Suspension Preparation Using the Arc Spray Nanoparticle Synthesis System Combined with Ultrasonic Vibration and Rotating Electrode. *The International Journal of Advanced Manufacturing Technology* 26: 552-558.

Choi, S. U. S., Z. G. Zhang, W. Yu, F. E. Lockwood, and E. A. Grulke (2001). Anomalous Thermal Conductivity Enhancement in Nanotube Suspensions. *Applied Physics Letters* 79: 2252-2254.

Chon, C. H., K. D. Kihm, S. P. Lee, and S. U. S. Choi (2005). Empirical Correlation Finding the Role of Temperature and Particle Size for Nanofluid (Al_2O_3) Thermal Conductivity Enhancement. *Applied Physics Letters* 87: 153107.

Chopkar, M, P. K. Das, and I. Manna. (2006) Synthesis and Characterization of a Nanofluid for Advanced Heat Transfer Applications. *Scripta Materialia* 55: 549-552.

Das, S. K., N. Putra, P. Thiesen, and W. Roetzel (2003a). Temperature Dependence of Thermal Conductivity Enhancement for Nanofluids. *Transactions of the ASME, Journal of Heat Transfer* 125: 567-574.

Das, S. K., N. Putra, and W. Roetzel (2003b). Pool Boiling Characteristics of Nano-Fluids. *International Journal of Heat and Mass Transfer* 46: 851-862.

Das, S. K., N. Putra, and W. Roetzel (2003c). Pool Boiling of Nano-Fluids on Horizontal Narrow Tubes. *International Journal of Multiphase Flow* 29: 1237-1247.

Davis, R. H. (1986). The Effective Thermal Conductivity of a Composite Material with Spherical Inclusions. *International Journal of Thermophysics* 7: 609-620.

De Bruijn, H. (1942). The Viscosity of Suspensions of Spherical Particles. *Recueil des travaux chimiques des Pays-Bas* 61: 863-874.

Ding, Y., and D. Wen (2005). Particle Migration in a Flow of Nanoparticle Suspensions. *Powder Technology* 149: 84-92.

Ding, Y., H. Alias, D. Wen, and R. A. Williams (2006). Heat Transfer of Aqueous Suspensions of Carbon Nanotubes (CNT nanofluids). *International Journal of Heat and Mass Transfer* 49: 240-250.

Dittus, F. W., and L. M. K. Boelter (1930). Heat Transfer in Automobile Radiators of the Tubular Type. *University of California Publications in Engineering*, 2: 443-461.

Eastman, J. A., S. U. S. Choi, S. Li, W. Yu, and L. J. Thompson (2001). Anomalous Increase in Effective Thermal Conductivity of Ethylene Glycol-Based Nanofluids Containing Copper Nanoparticles. *Applied Physics Letters* 78: 718-720.

Eilers, von H. (1941). Die Viskosität von Emulsionen hochviskoser Stoffe als Funktion der Konzentration. *Kolloid-Zeitschrift* 97: 313-321.

Einstein, A. (1906). Eine neue Bestimmung der Moleküldimensionen. *Annalen der Physik* 19: 289-306.

Eshelby, J. D. (1957). The Determination of the Elastic Field of an Ellipsoidal Inclusion, and Related Problems. *Proceedings of Royal Society of London A* 241: 376-396.

Evans, W., J. Fish, and P. Keblinski (2006). Role of Brownian Motion Hydrodynamics on Nanofluid Thermal Conductivity. *Applied Physics Letters* 88: 093116.

Faulkner, D. J., D. R. Rector, J. Davidson, and R. Shekarriz (2004). Enhanced Heat Transfer through the Use of Nanofluids in Forced Convection. *The Proceedings of IMECE 2004, Anaheim, California, USA, November 13-19, 2004*.

Frankel, N. A., and A. Acrivos (1967). On the Viscosity of Concentrated Suspension of Solid Spheres. *Chemical Engineering Science* 22: 847-853.

Fricke, H. (1924). A Mathematical Treatment of the Electric Conductivity and Capacity of Disperse Systems: I. The Electric Conductivity of a Suspension of Homogeneous Spheroids. *Physical Review* 24: 575-587.

Fricke, H. (1953). The Maxwell-Wagner Dispersion in a Suspension of Ellipsoids. *Journal of Physical Chemistry* 57: 934-937.

Gnielinski, V. (1976) New Equations for Heat and Mass Transfer in Turbulent Pipe and Channel Flow. *International Chemical Engineering* 16: 359-368.

Gosselin, L., and A. K. da Silva (2004). Combined "Heat Transfer and Power Dissipation" Optimization of Nanofluid Flows. *Applied Physics Letters* 85: 4160-4162.

Graham, A. L. (1981). On the Viscosity of Suspensions of Solid Spheres. *Applied Scientific Research* 37: 275-286.

Granqvist C. G., and R. A. Buhrman (1976). Ultrafine Metal Particles. *Journal of Applied Physics* 47: 22002219.

Granqvist, C. G., and O. Hunderi (1977). Optical Properties of Ultrafine Gold Particles. *Physical Review B* 16: 3513-3534.

Granqvist, C. G., and O. Hunderi (1978). Conductivity of Inhomogeneous Materials: Effective-Medium Theory with Dipole-Dipole Interaction. *Physical Review B* 18: 1554-1561.

Gupte, S. K., S. G. Advani, and P. Huq (1995). Role of Micro-Convection due to Non-Affine Motion of Particles in a Mono-Disperse Suspension. *International Journal of Heat and Mass Transfer* 38: 2945-2958.

Hamilton, R. L., and O. K. Crosser (1962). Thermal Conductivity of Heterogeneous Two-Component Systems. *Industrial & Engineering Chemistry Fundamentals* 1: 187-191.

Hasselman, D. P. H., and L. F. Johnson (1987). Effective Thermal Conductivity of Composites with Interfacial Thermal Barrier Resistance. *Journal of Composite Materials* 21: 508-515.

Henderson, J. R., and F. van Swol (1984). On the Interface between a Fluid and a Planar Wall: Theory and Simulations of a Hard Sphere Fluid at a Hard Wall. *Molecular Physics* 51: 991-1010.

Heris, S. Z., S. Gh. Etemad, and M. N. Esfahany (2006). Experimental Investigation of Oxide Nanofluids Laminar Flow Convective Heat Transfer. *International Communications in Heat and Mass Transfer* 33: 529-535.

Hong, T.-K., H.-S. Yang, and C. J. Choi (2005). Study of the Enhanced Thermal Conductivity of Fe Nanofluids. *Journal of Applied Physics* 97: 064311.

Hong, K. S., T.-K. Hong, and H.-S. Yang (2006). Thermal Conductivity of Fe Nanofluids Depending on the Cluster Size of Nanoparticles. *Applied Physics Letters* 88: 031901.

Hwang, Y., H. S. Park, J. K. Lee, and W. H. Jung (2006). Thermal Conductivity and Lubrication Characteristics of Nanofluids. *Current Applied Physics* 6S1: e67-e71.

Jang, S. P., and S. U. S. Choi (2004). Role of Brownian Motion in the Enhanced Thermal Conductivity of Nanofluids. *Applied Physics Letters* 84: 4316-4318.

Jeffrey, D. J. (1973). Conduction through a Random Suspension of Spheres. *The Proceedings of Royal Society of London A* 335: 355-367.

Jordan, A., R. Scholz, P. Wust, H. Föhling, and R. Felix (1999). Magnetic Fluid Hyperthermia (MFH): Cancer Treatment with AC Magnetic Field Induced Excitation of Biocompatible Superparamagnetic Nanoparticles. *Journal of Magnetism and Magnetic Materials* 201: 413-419.

Jou, R.-Y., and S.-C. Tzeng (2006). Numerical Research of Nature Convective Heat Transfer Enhancement Filled with Nanofluids in Rectangular Enclosures. *International Communications in Heat and Mass Transfer* 33: 727-736.

Kang, H. U., S. H. Kim, and J. M. Oh (2006). Estimation of Thermal Conductivity of Nanofluid Using Experimental Effective Particle Volume. *Experimental Heat Transfer* 19: 181-191.

Keblinski, P., and J. Thomin (2006). Hydrodynamic Field around a Brownian Particle. *Physical Review E* 73: 010502.

Kenneth S. S., M. Fang, and T. Hyeon (1996). Sonochemical Synthesis of Iron Colloids. *Journal of the American Chemical Society* 118: 11960-11961.

Kerner, E. H. (1956). The Electrical Conductivity of Composite Media. *The Proceedings of the Physical Society* B69: 802-807.

Khaled, A.-R. A., and K. Vafai (2005). Heat Transfer Enhancement through Control of Thermal Dispersion Effects. *International Journal of Heat and Mass Transfer* 48: 2172-2185.

Khanafer, K., K. Vafai, and M. Lightstone (2003). Bouyancy-Driven Heat Transfer Enhancement in a Two-Dimensional Enclosure Utilizing Nanofluids. *International Journal of Heat and Mass Transfer* 46: 3639-3653.

Kim, J., Y. T. Kang, and C. K. Choi (2004). Analysis of Convective Instability and Heat Transfer Characteristics of Nanofluids. *Physics of Fluids* 16: 2395-2401.

Kim, J., C. K. Choi, Y. T. Kang, and M. G. Kim (2006). Effects of Thermodiffusion Nanoparticles on Convective Instabilities in Binary Nanofluids. *Nanoscale and Microscale Thermophysical Engineering* 10: 29-39.

Koo, J., and C. Kleinstreuer (2004). A New Thermal Conductivity Model for Nanofluids. *Journal of Nanoparticle Research* 6: 577-588.

Koo, J., and C. Kleinstreuer (2005). Laminar Nanofluid Flow in Microheat-Sinks. *International Journal of Heat and Mass Transfer* 48: 2652-2661.

Krieger, I. M. (1972). Rheology of Monodisperse Lattices. *Advances in Colloid & Interface Sciences* 3: 111-136.

Kuhn, W., and H. Kuhn (1945). Die Abhängigkeit der Viskosität vom Strömungsgefälle bei hochverdünnten Suspensionen und Lösungen. *Helvetica Chimica Acta* 28: 97-127.

Kulkarni, D. P., D. K. Das, and G. A. Chukwu (2006). Temperature Dependent Rheological Property of Copper Oxide Nanoparticles Suspension (Nanofluid). *Journal of Nanoscience and Nanotechnology* 6: 1150-1154.

Kumar, D. H., H. E. Patel, V. R. R. Kumar, T. Sundararajan, T. Pradeep, and S. K. Das (2004). Model for Heat Conduction in Nanofluids. *Physical Review Letters* 93: 144301.

Kumar, S., and J. Y. Murthy (2005). A Numerical Technique for Computing Effective Thermal Conductivity of Fluid-Particle Mixtures. *Numerical Heat Transfer (Part B)* 47: 555-572.

Lamb, W., D. M. Wood, and N. W. Ashcroft (1978). Optical Properties of Small Particle Composites: Theories and Applications. In *Electrical Transport and Optical Properties of Inhomogeneous Media*, edited by J. C. Garland and D. B. Tanner: 240-255. New York: American Institute of Physics.

Landauer, R. (1952). The Electrical Resistance of Binary Metallic Mixtures. *Journal of Applied Physics* 23: 779-784.

Landauer, R. (1978). Electrical Conductivity in Inhomogeneous Media. In *Electrical Transport and Optical Properties of Inhomogeneous Media*, edited by J. C. Garland and D. B. Tanner: 2-43. New York: American Institute of Physics.

Lee, D., J.-W. Kim, and B. G. Kim (2006). A New Parameter to Control Heat Transport in Nanofluids: Surface Charge State of the Particle in Suspension. *Journal of Physical Chemistry B* 110: 4323-4328.

Lee, S., S. U.-S. Choi, S. Li, and J. A. Eastman (1999). Measuring Thermal Conductivity of Fluids Containing Oxide Nanoparticles. *Transactions of the ASME, Journal of Heat Transfer* 121: 280-289.

Li, C., M. Akinc, J. Wiench, M. Pruski, and C. H. Schilling (2005). Relationship between Water Mobility and Viscosity of Nanometric Alumina Suspensions. *Journal of the American Ceramic Society* 88: 2762-2768.

Li, C. H., and G. P. Peterson (2006). Experimental Investigation of Temperature and Volume Fraction Variations on the Effective Thermal Conductivity of Nanoparticle Suspensions (Nanofluids). *Journal of Applied Physics* 99: 084314.

Liu, M.-S., M. C.-C. Lin, I-T. Huang, C.-C. Wang (2005). Enhancement of Thermal Conductivity with Carbon Nanotube for Nanofluids. *International Communications in Heat and Mass Transfer* 32: 1202-1210.

Liu, M., M. Lin, C. Y. Tsai, C. Wang (2006). Enhancement of Thermal Conductivity with Cu for Nanofluids Using Chemical Reduction Method. *International Journal of Heat and Mass Transfer* 49: 3028-3033.

Liu, S., and J. H. Masliyah (1996). Rheology of Suspensions. In *Suspensions: Fundamentals and Applications in the Petroleum Industry*, edited by L. L. Schramm, American Chemical Society Advances in Chemistry Series 251: 107-176.

Liu, Z.-H., and Y.-H. Qiu (2006). Boiling Heat Transfer Characteristics of Nanofluids Jet Impingement on a Plate Surface. *Heat and Mass Transfer*, Springer: article in press (published online July 2006).

Lo, C.-H., T.-T. Tsung, L.-C. Chen, C.-H. Su, and H.-M. Lin (2005a). Fabrication of Copper Oxide Nanofluid Using Submerged Arc Nanoparticle Synthesis System (SANSS). *Journal of Nanoparticle Research* 7: 313-320.

Lo, C.-H., T.-T. Tsung, and L.-C. Chen (2005b). Shaped-Controlled Synthesis of Cu-Based Nanofluid Using Submerged Arc Nanoparticle Synthesis System (SANSS). *Journal of Crystal Growth* 277: 636-642.

Lu, S.-Y., and J.-L. Song (1996). Effective Conductivity of Composites with Spherical Inclusions: Effective of Coating and Detachment. *Journal of Applied Physics* 79: 609-618.

Lundgren, T. S. (1972). Slow Flow through Stationary Random Beds and Suspensions of Spheres. *Journal of Fluid Mechanics* 51: 273-299.

Ma, H. B., C. Wilson, B. Borgmeyer, K. Park, Q. Yu, S. U. S. Choi, and M. Tirumala (2006). Effect of Nanofluid on the Heat Transport Capability in an Oscillating Heat Pipe. *Applied Physics Letters* 88: 143116.

Maïga, S. E. B., C. T. Nguyen, N. Galanis, and G. Roy (2004). Heat Transfer Behaviours of Nanofluids in a Uniformly Heated Tube. *Superlattices and Microstructures* 35: 543-557.

Maïga, S. E. B., S. J. Palm, C. T. Nguyen, G. Roy, and N. Galanis (2005). Heat Transfer Enhancement by Using Nanofluids in Forced Convection Flows. *International Journal of Heat and Fluid Flow* 26: 530-546.

Mansour, R. B., N. Galanis, and C. T. Nguyen (2006). Effect of Uncertainties in Physical Properties on Forced Convection Heat Transfer with Nanofluids. *Applied Thermal Engineering* 27: 240-249.

Marquis, F. D. S., and L. P. F. Chibante (2005). Improving the Heat Transfer of Nanofluids and Nanolubricants with Carbon Nanotubes. *Journal of the Minerals, Metals & Materials Society* 57 (12): 32-43.

Masuda, H., A. Ebata, K. Teramae, and N. Hishinuma (1993). Alteration of Thermal Conductivity and Viscosity of Liquid by Dispersing Ultra-Fine Particles (Dispersion of γ -Al₂O₃, SiO₂, and TiO₂ Ultra-Fine Particles). *Netsu Bussei* 7: 227-233.

Maxwell, J. C. (1873). *Treatise on Electricity and Magnetism*. Oxford: Clarendon Press.

Milanova, D., and R. Kumar (2005). Role of Ions in Pool Boiling Heat Transfer of Pure and Silica Nanofluids. *Applied Physics Letters* 87: 233107.

Miles, J. B., Jr., and H. P. Robertson. (1932). The Dielectric Behavior of Colloidal Particles with an Electric Double-Layer. *Physical Review* 40: 583-591.

Mooney, M. (1951). The Viscosity of a Concentrated Suspension of Spherical Particles. *Journal of Colloid Science* 6: 162-170.

Murshed, S. M. S., K. C. Leong, and C. Yang (2005). Enhanced Thermal Conductivity of TiO₂-Water Based Nanofluids. *International Journal of Thermal Sciences* 44: 367-373.

Nan, C.-W., Z. Shi, and Y. Lin (2003). A Simple Model for Thermal Conductivity of Carbon Nanotube-Based Composites. *Chemical Physics Letters* 375: 666-669.

Nan, C.-W., G. Liu, Y. Lin, and M. Li (2004). Interface Effect on Thermal Conductivity of Carbon Nanotube Composites. *Applied Physics Letters* 85: 3549-3551.

Pak, B. C., and Y. I. Cho (1998). Hydrodynamic and Heat Transfer Study of Dispersed Fluids with Submicron Metallic Oxide Particles. *Experimental Heat Transfer* 11: 151-170.

Patel, H. E., S. K. Das, T. Sundararajan, A. S. Nair, B. George, and T. Pradeep (2003). Thermal Conductivity of Naked and Monolayer Protected Metal Nanoparticle Based Nanofluids: Manifestation of Anomalous Enhancement and Chemical Effects. *Applied Physics Letters* 83: 2931-2933.

Pauly, von H., and H. P. Schwan (1959). Über die Impedanz einer Suspension von kugelförmigen Teilchen mit einer Schale. *Zeitschrift für Naturforschung* 146: 125-131.

Phan-Thien, N., and A. L. Graham (1991). A New Constitutive Model for Fibre Suspensions: Flow past a Sphere. *Rheologica Acta* 30: 44-57.

Polder, D., and J. H. van Santen (1946). The Effective Permeability of Mixtures of Solids. *Physica* 12: 257-271.

Pozhar, L. A. (2000). Structure and Dynamics of Nanofluids: Theory and Simulations to Calculate Viscosity. *Physical Review E* 61: 1432-1446.

Prasher, R., P. Bhattacharya, and P. E. Phelan (2005). Thermal Conductivity of Nanoscale Colloidal Solutions (Nanofluids). *Physical Review Letters* 94: 025901.

Prasher, R., P. Bhattacharya, and P. E. Phelan (2006a). Brownian-Motion-Based Convective-Conductive Model for the Thermal Conductivity of Nanofluids. *Transaction of the ASME, Journal of Heat Transfer* 128: 588-595.

Prasher, R., P. E. Phelan, and P. Bhattacharya (2006b). Effect of Aggregation Kinetics on the Thermal Conductivity of Nanoscale Colloidal Solutions (Nanofluid). *Nano Letters* 6: 1529-1534.

Prasher, R., W. Evans, P. Meakin, J. Fish, P. Phelan, and P. Keblinski (2006c). Effect of Aggregation on Thermal Conduction in Colloidal Nanofluids. *Applied Physics Letters* 89: 143119.

Putnam, S. A., D. G. Cahill, P. V. Braun, Z. Ge, and R. G. Shimmin (2006). Thermal Conductivity of Nanoparticle Suspensions. *Journal of Applied Physics* 99: 084308.

Putra, N., W. Roetzel, and S. K. Das (2003). Natural Convection of Nano-Fluids. *Heat and Mass Transfer* 39: 775-784.

Rayleigh, L. (1892). On the Influence of Obstacles Arranged in Rectangular Order upon the Properties of a Medium. *Philosophical Magazine* 34: 481-502.

Ren, Y., H. Xie, and A. Cai (2005). Effective Thermal Conductivity of Nanofluids Containing Spherical Nanoparticles. *Journal of Physics D: Applied Physics* 38: 3958-3961.

Robinson, J. V. (1949). The Viscosity of Suspensions of Spheres. *Journal of Physical & Colloid Chemistry* 53: 1042-1056.

Romano, J. M., J. C. Parker, and Q. B. Ford (1997). Application Opportunities for Nanoparticles Made from Condensation of Physical Vapor. *Advances in Powder Metallurgy and Particulate Materials* 2: 12-3.

Roscoe, R. (1952). The Viscosity of Suspensions of Rigid Spheres. *British Journal of Applied Physics* 3: 267-269.

Routbort, J. L., and D. Singh (2006). Erosion of Materials in Nanofluids. In the U.S. Department of Energy Annual Progress Report: Heavy Vehicle Systems Optimization Program.

Roy, G., C. T. Nguyen, and P. Lajoie (2004). Numerical Investigation of Laminar Flow and Heat Transfer in a Radial Flow Cooling System with the Use of Nanofluids. *Superlattices and Microstructures* 35: 497-511.

Saitô, N. (1950). Concentration Dependence of the Viscosity of High Polymer Solutions. I. *Journal of the Physical Society of Japan* 5: 4-8.

Sato, Y., E. Deutsch, and O. Simonin (1998). Direct Numerical Simulations of Heat Transfer by Solid Particles Suspended in Homogeneous Isotropic Turbulence. *International Journal of Heat and Fluid Flow* 19: 187-192.

Schwan, H. P., G. Schwarz, J. Maczuk, and H. Pauly (1962). On the Low-Frequency Dielectric Dispersion of Colloidal Particles in Electrolyte Solution. *Journal of Physical Chemistry* 66: 2626-2635.

Shenogin, S., L. Xue, R. Ozisik, P. Keblinski, and D. G. Cahill (2004). Role of Thermal Boundary Resistance on the Heat Flow in Carbon-Nanotube Composites. *Journal of Applied Physics* 95: 8136-8144.

Simha, R. (1940). The Influence of Brownian Movement on the Viscosity of Solutions. *Journal of Physical Chemistry* 44: 25-34.

Simha, R. (1952). A Treatment of the Viscosity of Concentrated Suspensions. *Journal of Applied Physics* 23: 1020-1024.

Srdić, V. V., M. Winterer, A. Möller, G. Miehe, and H. Hahn (2001). Nanocrystalline Zirconia Surface-Doped with Alumina: Chemical Vapor Synthesis, Characterization, and Properties. *Journal of the American Ceramic Society* 84: 2771-2776.

Tsai, C. Y., H. T. Chien, P. P. Ding, B. Chan, T. Y. Luh, and P. H. Chen (2004). Effect of Structural Character of Gold Nanoparticles in Nanofluid on Heat Pipe Thermal Performance. *Materials Letters* 58: 1461-1465.

Taylor, L. S. (1965). Dielectrics Properties of Mixtures. *IEEE Transactions on Antennas and Propagation AP-13*: 943-947.

Taylor, L. S. (1966). Dielectrics Loaded with Anisotropic Materials. *IEEE Transactions on Antennas and Propagation AP-14*: 669-670.

Tseng, W. J., and K.-C. Lin (2003). Rheology and Colloidal Structure of Aqueous TiO₂ Nanoparticle Suspensions. *Materials Science and Engineering A* 355: 186-192.

Tzeng, S.-C., C.-W. Lin, and K. D. Huang (2005). Heat Transfer Enhancement of Nanofluids in Rotary Blade Coupling of Four-Wheel-Drive Vehicles. *Acta Mechanica* 179: 11-23.

Van de Hulst, H. C. (1957). *Light Scattering by Small Particles*. New York: John Wiley & Sons.

Vand, V. (1948). Viscosity of Solutions and Suspensions. I. Theory. *Journal of Physical and Colloid Chemistry* 52: 277-299.

Vassallo, P., R. Kumar, and S. D'Amico (2004). Pool Boiling Heat Transfer Experiments in Silica-Water Nano-Fluids. *International Journal of Heat and Mass Transfer* 47: 407-411.

Wang, B.-X., L.-P. Zhou, and X.-F. Peng (2003). A Fractal Model for Predicting the Effective Thermal Conductivity of Liquid with Suspension of Nanoparticles. *International Journal of Heat and Mass Transfer* 46: 2665-2672.

Wang, X., X. Xu, and S. U. S. Choi (1999). Thermal Conductivity of Nanoparticle-Fluid Mixture. *Journal of Thermophysics and Heat Transfer* 13: 474-480.

Wen, D., and Y. Ding (2004a). Experimental Investigation into Convective Heat Transfer of Nanofluids at the Entrance Region under Laminar Flow Conditions. *International Journal of Heat and Mass Transfer* 47: 5181-5188.

Wen, D., and Y. Ding (2004b). Effective Thermal Conductivity of Aqueous Suspensions of Carbon Nanotubes (Carbon Nanotube Nanofluids). *Journal of Thermophysics and Heat Transfer* 18: 481-485.

Wen, D., and Y. Ding (2005a). Effect of Particle Migration on Heat Transfer in Suspensions of Nanoparticles Flowing through Minichannels. *Microfluid Nanofluid* 1: 183-189.

Wen, D., and Y. Ding (2005b). Experimental Investigation into the Pool Boiling Heat Transfer of Aqueous Based γ -Alumina Nanofluids. *Journal of Nanoparticle Research* 7: 265-274.

Wen, D., and Y. Ding (2005c). Formulation of Nanofluids for Natural Convective Heat Transfer Applications. *International Journal of Heat and Fluid Flow* 26: 855-864.

Wen, D., and Y. Ding (2006). Natural Convective Heat Transfer of Suspensions of Titanium Dioxide Nanoparticles (Nanofluids). *IEEE Transactions on Nanotechnology* 5: 220-227.

Wiener, O. (1912). Die Theorie des Mischkörpers für das Feld der stationären Strömung. 1. Abhandlung: Die Mittelwertsätze für Kraft, Polarisierung und Energie. *Der Abhandlungen der Mathematisch-Physischen Klasse der Königlich Sächsischen Gesellschaft der Wissenschaften* 32: 507-604.

Xie, H., J. Wang, T. Xi, and Y. Liu (2002a). Thermal Conductivity of Suspensions Containing Nanosized SiC Particles. *International Journal of Thermophysics* 23: 571-580.

Xie, H., J. Wang, T. Xi, and F. Ai (2002b). Thermal Conductivity Enhancement of Suspensions Containing Nanosized Alumina Particles. *Journal of Applied Physics* 91: 4568-4572.

Xie, H., J. Wang, T. Xi, Y. Liu, and F. Ai (2002c). Dependence of the Thermal Conductivity of Nanoparticle-Fluid Mixture on the Base Fluid. *Journal of Materials Science Letters* 21: 1469-1471.

Xie, H., H. Lee, W. Youn, and M. Choi (2003). Nanofluids Containing Multiwalled Carbon Nanotubes and Their Enhanced Thermal Conductivities. *Journal of Applied Physics* 94: 4967-4971.

Xie, H., M. Fujii, and X. Zhang (2005). Effect of Interfacial Nanolayer on the Effective Thermal Conductivity of Nanoparticle-Fluid Mixture. *International Journal of Heat and Mass Transfer* 48: 2926-2932.

Xuan, Y., and Q. Li (2000). Heat Transfer Enhancement of Nanofluids. *International Journal of Heat and Fluid Flow* 21: 58-64.

Xuan, Y., and Q. Li (2003). Investigation on Convective Heat Transfer and Flow Features of Nanofluids. *Transactions of the ASME, Journal of Heat Transfer* 125: 151-155.

Xuan, Y., Q. Li, and W. Hu (2003). Aggregation Structure and Thermal Conductivity of Nanofluids. *AIChE Journal* 49 (4): 1038-1043.

Xuan, Y., and Z. Yao (2005). Lattice Boltzmann Model for Nanofluids. *Heat and Mass Transfer* 41: 199-205.

Xue, L., P. Keblinski, S. R. Phillpot, S. U.-S. Choi, and J. A. Eastman (2004). Effect of Liquid Layering at the Liquid-Solid Interface on Thermal Transport. *International Journal of Heat and Mass Transfer* 47: 4277-4284.

Xue, Q. (2000). Effective-Medium Theory for Two-Phase Random Composite with an Interfacial Shell. *Journal of Material Science and Technology* 16: 367-369.

Xue, Q. Z. (2005). Model for Thermal Conductivity of Carbon Nanotube-Based Composites. *Physica B* 368: 302-307.

Yang, Y., Z. G. Zhang, E. A. Grulke, W. B. Anderson, and G. Wu (2005). Heat Transfer Properties of Nanoparticle-in-Fluid Dispersions (Nanofluids) in Laminar Flow. *International Journal of Heat and Mass Transfer* 48: 1107-1116.

Yang, B., and Z. H. Han (2006). Temperature-Dependent Thermal Conductivity of Nanorod-Based Nanofluids. *Applied Physics Letters* 89: 083111.

Yang, Y., E. A. Grulke, Z. G. Zhang, and G. Wu (2006). Thermal and Rheological Properties of Carbon Nanotube-in-Oil Dispersions. *Journal of Applied Physics* 99:114307.

You, S. M., J. H. Kim, and K. H. Kim (2003). Effect of Nanoparticles on Critical Heat Flux of Water in Pool Boiling Heat Transfer. *Applied Physics Letters* 83: pp. 3374-3376.

Yu, C.-J., A. G. Richter, A. Datta, M. K. Durbin, and P. Dutta (2000). Molecular Layering in a Liquid on a Solid Substrate: an X-Ray Reflectivity Study. *Physica B* 283: 27-31.

Yu, W., and S. U. S. Choi (2003). The Role of Interfacial Layers in the Enhanced Thermal Conductivity of Nanofluids: A Renovated Maxwell Model. *Journal of Nanoparticle Research* 5: 167-171.

Yu, W., and S. U. S. Choi (2004). The Role of Interfacial Layers in the Enhanced Thermal Conductivity of Nanofluids: A Renovated Hamilton-Crosser Model. *Journal of Nanoparticle Research* 6: 355-361.

Yu, W., and S. U. S. Choi (2005). An Effective Thermal Conductivity Model of Nanofluids with a Cubic Arrangement of Spherical Particles. *Journal of Nanoscience and Nanotechnology* 5: 580-586.

Zhang, Z., and Q. Que (1997). Synthesis, Structure and Lubricating Properties of Dialkyldithiophosphate-Modified Mo-S Compound Nanoclusters. *Wear* 209: 8-12.

Zhu, H.-T., Y.-S. Lin, and Y.-S. Yin (2004). A Novel One-Step Chemical Method for Preparation of Copper Nanofluids. *Journal of Colloid and Interface Science* 277: 100-103.



Energy Systems Division

Argonne National Laboratory
9700 South Cass Avenue, Bldg. 212
Argonne, IL 60439-4838

www.anl.gov



UChicago ►
Argonne_{LLC}

A U.S. Department of Energy laboratory
managed by UChicago Argonne, LLC